Encapsulation of Organic Light Emitting Diodes

Bhadri Visweswaran

A Dissertation
Presented to the Faculty
of Princeton University
in Candidacy for the Degree
of Doctor of Philosophy

Recommended for Acceptance
by the Department of
Electrical Engineering
Adviser: Professor Sigurd Wagner

November 2014

Abstract

Organic Light Emitting Diodes (OLEDs) are extremely attractive candidates for flexible display and lighting panels due to their high contrast ratio, light weight and flexible nature. However, the materials in an OLED get oxidized by extremely small quantities of atmospheric moisture and oxygen. To obtain a flexible OLED device, a flexible thin-film barrier encapsulation with low permeability for water is necessary.

Water permeates through a thin-film barrier by 4 modes: microcracks, contaminant particles, along interfaces, and through the bulk of the material. We have developed a flexible barrier film made by Plasma Enhanced Chemical Vapor Deposition (PECVD) that is devoid of any microcracks. In this work we have systematically reduced the permeation from the other three modes to come up with a barrier film design for an operating lifetime of over 10 years.

To provide quantitative feedback during barrier material development, techniques for measuring low diffusion coefficient and solubility of water in a barrier material have been developed. The mechanism of water diffusion in the barrier has been identified. From the measurements, we have created a model for predicting the operating lifetime from accelerated tests when the lifetime is limited by bulk diffusion.

To prevent the particle induced water permeation, we have encapsulated artificial particles and have studied their cross section. A three layer thin-film that can coat a particle at thicknesses smaller than the particle diameter is identified. It is demonstrated to protect a bottom emission OLED device that was contaminated with standard sized glass beads.

The photoresist and the organic layers below the barrier film causes sideways permeation that can reduce the lifetime set by permeation through the bulk of the barrier. To prevent the sideways permeation, an impermeable inorganic grid made of the same barrier material is designed. The reduction in sideways permeation due to the impermeable inorganic grid is demonstrated in an encapsulated OLED.

In this work, we have dealt with three permeation mechanisms and shown solution to each of them. These steps give us reliable flexible encapsulation that has a lifetime of greater than 10 years.

Acknowledgements

I have been blessed with incredible teachers, colleagues and friends at Princeton. Words cannot begin to describe their contribution. I would like to begin with my incredible advisor Professor Sigurd Wagner. He is a great teacher and mentor from whom I have learned a lot both academically and professionally. I sincerely thank him for his advice through these years. I would like to thank Professor James Sturm for providing inputs and encouragement throughout the research program. I thank him for setting ambitious targets and providing innumerable ideas for carrying out research. I would like to thank Professor Barry Rand and Professor George Scherer for reading my thesis and providing valuable comments. I would like to thank Professor Antoine Kahn for his inputs over the past five years.

I would like to thank Professor Samuel Cohen and Princeton Plasma Science and Technology for awarding fellowships through the graduate program. My collaborators at Universal Display Corporation, Ray Ma, Siddharth Harikrishna Mohan, Prashant Mandlik, William Quinn and Jeff Silvernail had put faith in my capabilities three years ago and funded this work. I thank for the amazing technical and intellectual support I received from them. I would like to specially mention Siddharth Harikrishna Mohan and Prashant Mandlik for providing me with samples with great enthusiasm. Thanks to Ray Ma for providing valuable advice in choosing my career path. I would like to express my gratitude to the members of the UDC community, who have supported my research.

My parents are the sole reason I was able to come to Princeton. They are tiger parents who put my and my sister's priorities above theirs. This doctoral degree has come to fruition because of your dreams. Rhama, you are an amazing sister. Thank you being excited about my work and life.

I would like to thank my undergraduate advisor Professor V. K. Chaubey for encouraging me to join the graduate program at Princeton. Yifei Huang and Ting Liu, you taught me to use the PECVD, a beast of an equipment. Yifei, I attribute my knowledge in maintaining the lab and fixing equipment to your training. It was incredible fun when you were around. Ting, we spent a lot of time in the lab working on the PECVD. I had loads of fun and the lab has not been the same since your graduation. I would like to thank you for guiding me through my general exam. Thank you for being sharp and strong in providing comments on my graduate work ethic and at the same time being amazingly funny and joyful. I missed your absence in the lab after your graduation.

Sushobhan Avasthi, the wise man, the meat of this thesis is on experiments that arose from conversations with you. I pin my successful graduate program on these conversations. Your selfless approach in helping me and other graduate students in their respective work stands second to none. You are going to be an amazing Professor. Lin Han, thank you for training me on encapsulation PECVD. The entire background work for my thesis originates from it. Warren you are the best student and colleague to I have ever had. You are more than willing to learn and give your best in helping others needs. I am extremely thankful to use and maintain the PECVD alongside with you. I would like to express my thanks to you for taking initiative in keeping the lab running smooth. Josh, thank you for all the fun time we had in the lab. I will never forget your quirks.

Dolly, words cannot begin to describe your part in my life during my stay at Princeton. You are a thoughtful, wonderful and sweet person and thank you for adding a vibrant color to my life at Princeton. Chiao-Ti, thank your for helping me out in the lab with equipment. Arvind, I have known you for 10 years as a super awesome best friend and this is an appropriate moment to thank you for all your support and guidance. Ken, Joseph, Amy, Tiffany and Yasmin, thanks for helping me in the lab, be it cleaning the lab floor or fixing a leaky pipe. Thanks for your support. Jerry Poirier and Nan Yao, your training and assistance in the SEM cannot be thanked enough. The fruits of my experiments directly originate from the SEM images that I took with your help. Kevin Loutherback, my bike/ski buddy we have had good times. Thanks for teaching me how to ski and introducing me to the world of biking. I hope we have lot more bike and ski rides together in the bay area. Sonika Johri, Carole Dalin, Dan Wright, Maika Takita, Loren Alegria, Quentin Berthert, David McGady and Joe Benoit my fellow 96mountaineers cheers to the good times we had at mountain ave. It was an incredible journey at home. Carole I have learnt quite a bit from you. Thank you and I hope we stay in touch. Devin, you are wise man and a great teacher. When I came to the United States, you taught me the way of life here. We have ski'ed, biked, swimmed, wake boarded, played board games. You introduced me to all these fun activities and sports. Thanks for looking out always. Curt Schieler, I am going to miss the board game evenings. Jimmy Belasco thanks for all the fun parties where we hung out at. Stefan Munzel, Andrew Shu, Ryan Jock, David Eis and Celine Stein we have come a long way having loads of fun for the past five years. Mad Raman, your crazy theories are always enlightening. We shall meet in the bay area. Arjun Vijay, your punch lines are out of the world. No one can beat them. Special thanks to Challa Abhishek for giving wise advice at the right moments. I have to thank all my wingies and non-wingies in BITS who have been super fun and supportive.

This acknowledgement is neither complete with the list of people not their contributions. I could write a whole thesis on my friends and family that helped me get where I am.

Thank you all!

To my teachers.

Contents

List of Tables

List of Figures

Chapter 1

Introduction

Organic Light Emitting Diodes (OLEDs) have been introduced in flat panel displays, handheld devices, phones and lighting. OLEDs are very attractive semiconductors in terms of visual appearance, efficiency and mechanical flexibility[1, 2]. But they have the drawback of being unstable upon exposure to moisture and air. Extremely small quantities of water can corrode the low-work function cathode, de-activate the emissive organic molecules and oxidize the metal-organic interface[3]. In today's rigid displays, the OLED is encapsulated together with a desiccant between two glass plates that are edge-sealed with a polymeric sealant[4] as illustrated figure 1.1a. While glass plates are excellent permeation barriers, they are rigid. Flexible glass sheets, which are thinner than 100 µm, have not yet entered display use. To make a display flexible, the bottom and top glass plates are replaced by a flexible substrate and a flexible encapsulation. The flexible substrate is made of polymers that allow water to permeate. Typically the substrate is coated with a flexible barrier, the OLED is fabricated on it, and then the OLED in turn is coated with a flexible barrier; a foil of plastic is laminated with an adhesive over the top for mechanical protection and mechanical stress compensation[5]. The flexible barrier film prevents the permeation of water into the OLED. Figure 1.1b is the schematic of such a structure.

The least-permeable and optically clear barrier materials are $\mathrm{SiO_2}$, $\mathrm{SiN_x}$, and $\mathrm{Al_2O_3}$. However, when these materials are deposited as thin films in order to be flexible, they develop microcracks[6, 7] that render the films permeable. In addition, particulate contamination break the integrity of the barrier films[8, 9, 10]. In the conventional approach to solving these problems, alternating polymer

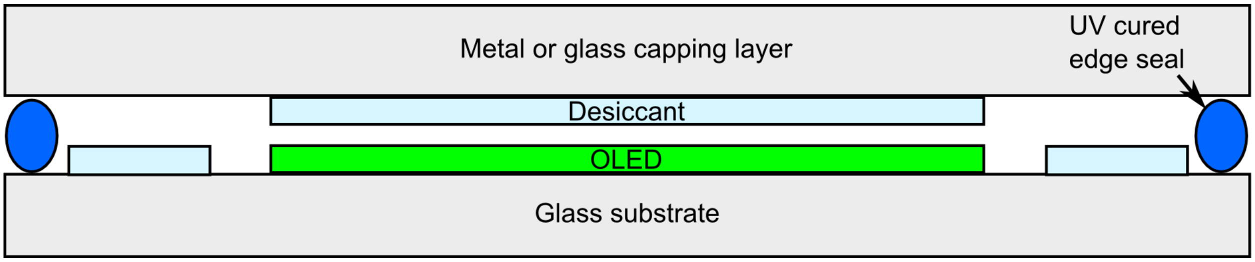

(a) Glass encapsulation of OLED. The OLED is sandwiched between a glass substrate and a glass or metal cap along with desiccant.

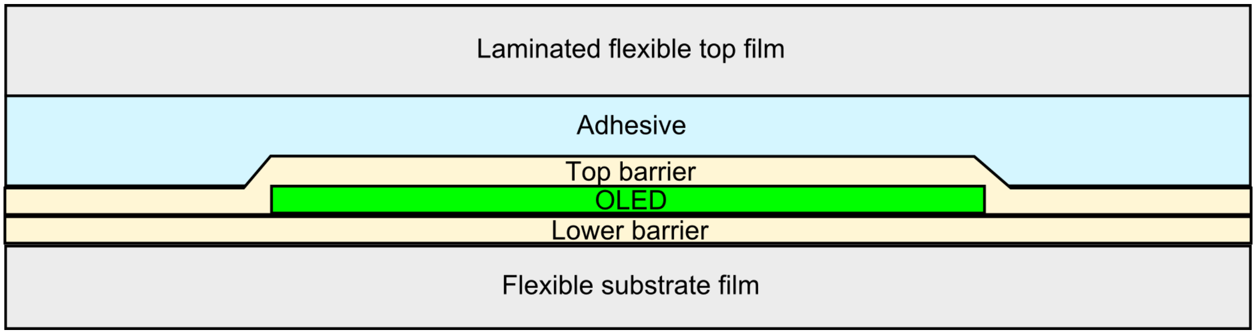

(b) The OLED is deposited on a flexible substrate with barrier film. A top barrier film is deposited on top of the OLED in an OLED compatible low temperature process. A flexible film is laminated on top of the top barrier film with adhesive to physically protect the barrier film and keep the film in the neutral plane while bending.

Figure 1.1: Encapsulation techniques for packaging Organic Light Emitting Diodes to prevent reactive degradation upon exposure to atmospheric moisture and oxygen.

layers and inorganic layers are deposited[11, 12, 13]. The polymer layers mechanically decouple the adjacent inorganic layers. In particular they decouple their microcracks such that microcracks in nearest-neighbour inorganic layers are not aligned with each other. The ensuing misalignment of microcracks makes the diffusion path for permeating atmospheric gas molecules very long. The polymers layers and the inorganic/polymer interfaces also can function as desiccants. Long diffusion paths combined with desiccation protects the OLED adequately[14]. Fabrication in this case is expensive due to the requirement of multiple deposition steps.

To reduce the time taken for film fabrication, we have been developing a single process barrier material that has very low permeability yet forms mechanically flexible and conformal films[15]. The material is a SiO_2-silicone *hybrid* that is deposited by plasma-enhanced chemical vapor deposition (PECVD) from the source gases hexamethyldisiloxane (HMDSO) and oxygen. The properties of this hybrid material can be varied from SiO_2-like to silicone polymer-like, by varying the flow rates of HMDSO and oxygen and the radio frequency power that is fed into the glow discharge[16]. This thesis describes the steps we have taken to creating long-lasting barrier film out of this barrier material.

1.1 OLED WVTR requirement

The performance of a barrier film is traditionally defined by its water vapor transmission rate, WVTR and oxygen transmission rate, OTR. WVTR is the amount of water that permeates across a barrier that protects the OLED. Its low work function cathode is easily oxidized by water[17] and the organic emissive layers can form defect states upon water exposure that quench emission[18]. This results in OLED degradation. A barrier film prevents degradation by preventing the water from reaching the OLED. A commonly accepted yet debatable value for upper limit value for WVTR to protect OLEDs for over several years is 10^{-6} g/m^2/day[5, 19]. Figure 1.2 is a chart illustrating the range of water vapor transmission rates and oxygen transmission rates required for protection in different applications. In an OLED display or a lighting panel, the exact WVTR requirement is determined by the design of OLED and the expected device shelf lifetime.

1.2 Modes of permeation of water in a barrier film

Bulk inorganic materials such as SiN_x or Al_2O_3 are impermeable to water. Ideally, a very thin layer, less than 100 nm of bulk inorganic material should have water vapor transmission rate less than 10^{-6} g/m^2/day. But, when the barrier film is deposited through PECVD or sputter deposition as a thin-film, the barrier does not behave as its bulk form. It has pin-holes, embedded particles and weak interfaces with the substrate which introduce pathways for water. Such pathways for water lead to the failure of a moisture sensitive device. This section describes the different modes of permeation in a thin-film and its impact on the device failure. Figure 1.3 illustrates the different modes of water permeation in a barrier film and they are:

1.2.1 Permeation through microdefects

Inorganic materials in the form of thin-films are prone to microdefects[22]. Microdefects include pin-holes, grain boundaries and microcracks. In thin-films the microdefects often run between the

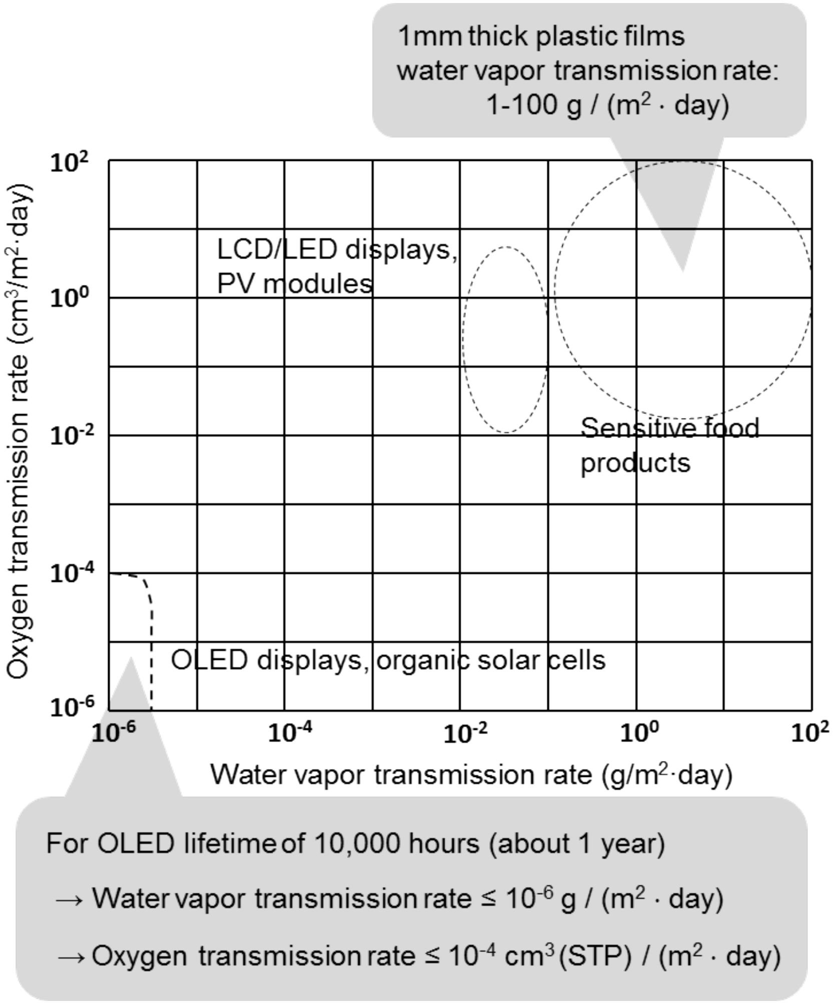

Figure 1.2: OLEDs demand a water vapor transmission rates $\leq 10^{-6}$ g/m^2/day. Liquid crystal displays[20, 21], photovoltaic modules and food packaging[22] are less sensitive to moisture and oxygen[23].

two faces of the film. As a result in thin-films they act as pathways for water and oxygen to permeate from one face to another. The microdefects that run between the two faces of the barrier film have to be eliminated to achieve encapsulation.

1.2.2 Break in encapsulation due to particles

The presence of particles on the surface of the OLED after evaporation of organic emissive layers and metal cathode is inevitable. The particles arise from the walls of the deposition chambers and/or deposition processes themselves. The barrier deposition process itself may generate particles. The presence of particles on the surface of the OLED with particle size comparable to the size of the

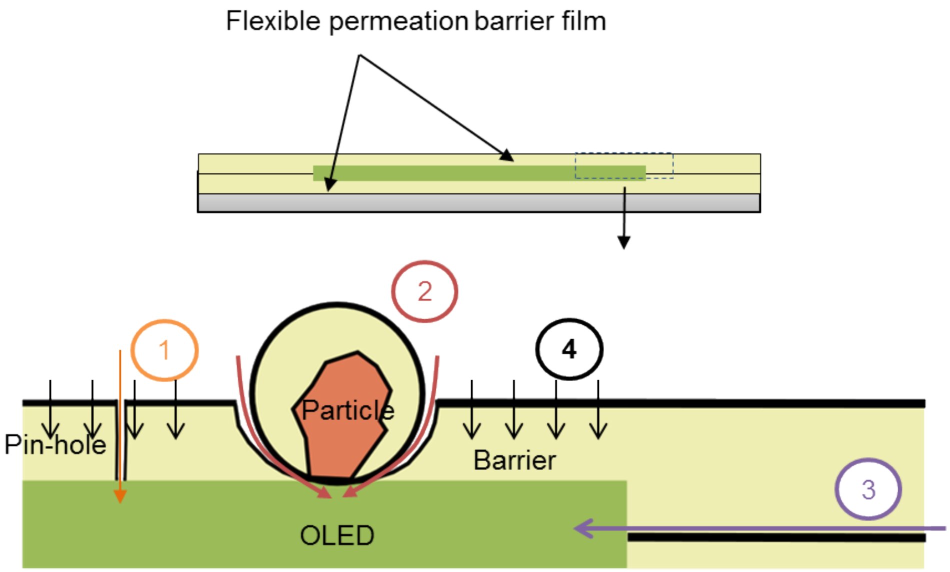

Figure 1.3: A barrier film has four modes of permeation: 1. through microdefects, 2. through breaks in encapsulation caused by particles, 3. sideways permeation along the interface between barrier and substrate. 4. by diffusion through the *bulk* of the barrier film[24].

barrier film will break the continuity of the barrier film. This results in a direct pathways for the water to permeate from the ambient and reach the OLED. Pathway #2 in figure 1.3 is an illustration of a break in the barrier film due to a particle.

To avoid such particle problem, a thick barrier film can be employed that will completely bury the particle. But, thick films have the disadvantage of needing long deposition times (hence being costly) and being more rigid. In the case of a multilayer barrier film, the number of layers have to be increased. This results in long deposition times and a barrier film that is less flexible. To overcome these disadvantages, barrier films that are thinner than the size of the particle but yet at the same time can completely encapsulate it need to be identified. Particle encapsulation of the barrier film is analyzed in detail in chapter 6.

Figure 1.4 shows two examples of encapsulation results, to explain particle induced failure. A 6 µm thick barrier film encapsulates and protects OLEDs for several thousand hours, whereas a 4 µm thick film shows a growing black spot in few tens of hours at high temperature and humidity test conditions[25][1]. In both films, particles are expected to be present on the surface of the OLED. While the 6 µm film completely buried particles, the 4 µm film did not, leading to rapid failure by

---

[1] Barrier lifetime is equal to OLED device shelf lifetime. OLED devices require a shelf life of 10 years at room temperature conditions. High temperature and relative humidity accelerates water permeation. 1000 hours = 42 days.

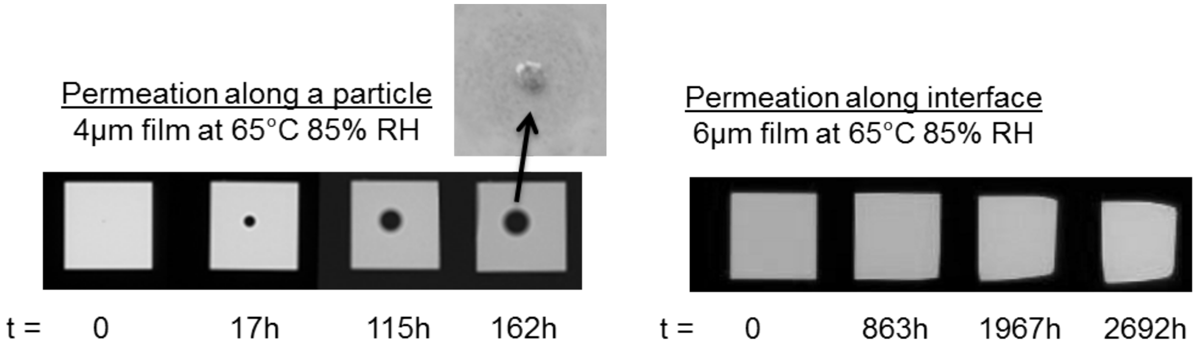

(a) A 4 μm thick barrier film encapsulating an OLED pixel. A black spot is observed at 17 hours at 65 °C 85% relative humidity due to the presence of a particles (pathway #2 in fig 1.3). The top image in the inset shows the SEM image taken of the particle that is 4 μm in size.

(b) A 6 μm thick barrier film encapsulating an OLED pixel. The degradation is found on the pixel after several thousand hours of testing results from sideways permeation of water from the edge of the encapsulation that causes shrinkage of the pixels (pathway #3 in fig 1.3).

Figure 1.4: A thickness change from 4 μm to 6 μm of the encapsulating barrier film increases the lifetime of the device by orders of magnitude[25].

top-to-bottom permeation. The inset shows an SEM image of a 4 μm particle that is the source of defect in the device encapsulated with the thinner film. The particle breaks the continuity of the barrier film dramatically reducing the OLED lifetime.

The break in encapsulation in the barrier either due to particles or due to micro-defects is termed under an umbrella term as a *defect*.

1.2.3 Sideways permeation

Figure 1.4b is an example for the OLED pixel is shrinking in size due to sideways interface permeation. Sideways permeation water is caused by weak interfaces between the barrier film and substrate or permeable organic layers adjacent to the pixel. If there is a break in encapsulation outside of the OLED luminescent area, water entering through this defect may permeate sideways into the OLED, causing shrinkage. This sideways permeation and its relevance to reliability of OLED lifetime prediction is discussed in detail in chapter 9 and 10. The width of the bezel in a display is also determined by the rate of sideways permeation.

1.2.4 Bulk permeation in a material

Water and oxygen permeates through the bulk of organic and certain inorganic materials. Polymers and organic materials typically show very high permeation for water. As a result, a standalone polymer or organic film cannot be used as a barrier to encapsulate an OLED. Even if the polymer film coats conformally without any break in encapsulation due to particles, the bulk permeation would be so high that it would result in the degradation of the OLED emissive layers and the cathode layers. Pathway #4 in figure 1.3 shows such bulk permeation in a barrier film. Inorganic films are less permeable. During experimentation with our *hybrid* silicon dioxide-silicone barrier, measurement of bulk permeation is necessary to evaluate the quality of the barrier material.

1.3 Bottleneck in developing a barrier film

Encapsulated OLEDs are stored at elevated temperature and humidity in an environmental test chamber to evaluate the barrier film's performance. High temperature and relative humidity accelerate water induced degradation of the OLED. Typical conditions used for acceleration are 85 °C and 85% relative humidity, 65 °C and 90% relative humidity and 60 °C and 90% relative humidity. The OLEDs under test are turned on periodically to check for any OLED degradation. When dark spots or bands appear in the luminescent area, the OLED is considered to have failed and the time of failure is defined as the *lifetime*. Typical targets for OLED lifetime in such accelerated tests are 500 or 1,000 hours [see section 4.6 for extraction of lifetime under actual operating condition from accelerated tests]. If an OLED shows no dark spot or band at the end of this period, the encapsulation capability is considered to be adequate.

This lifetime test, conducted directly on encapsulated OLEDs, has a great advantage: it is highly sensitive and it is realistic because it is conducted directly on the device that is to be protected. But it has two drawbacks. One is that the tests take three to six weeks, or even longer[15] to identify the lifetime. This long delay between OLED encapsulation and test results seriously slows down experiments on new or modified barrier materials and the evaluation of their applicability to OLED encapsulation. A second disadvantage is that the OLED dark spots or bands do not distinguish clearly between the three pathways by which water can reach an encapsulated OLED (figure 1.3).

Because the lifetime tests do not inform about the inherent permeability of a barrier material, it cannot be used to efficiently guide material optimization. The same disadvantage applies to a similarly sensitive test in which permeation is detected by the bleaching of an underlying reflective film of metallic calcium[26].

In a group of widely employed tests a gas or water vapor is allowed to permeate across a free standing barrier film. The flux of permeating gas is measured[27] and the permeability of the barrier film is defined. But these tests are not sufficiently sensitive and also cannot discriminate between the three permeation mechanisms. With the exception of expensive ion beam techniques such as secondary ion mass spectrometry (SIMS) and helium ion backscattering, none of the existing techniques can measure water permeation through the bulk of a barrier material at the level of sensitivity that OLEDs demand.

Figure 1.4 is a classic example where two OLED samples deposited with two barrier films of the same kind but with different thickness have been fabricated on an OLED that have been subject to an environmental test, but reveals very little quantitative information. Using such environmental tests, the true lower limit for thickness can never be identified for the barrier material unless all particles have been eliminated. But removing particles is nearly impossible to do in a research environment. Characterization techniques that are immune to the presence of particles are required to evaluate the permeation properties of a material.

The presence of particles during research and development impedes material characterization and tremendously reduces the pace of barrier film development. Barrier material characterization techniques insensitive to particles and defects need to be performed alongside the efforts of getting rid of most of the particles. In the end all devices should have all particles either eliminated or encapsulated. In a situation where there is a fraction of devices in which particles have not been encapsulated, those devices need to be identified discarded (see section 9.3).

1.4 Aim

The aim is to achieve a sub-5 μm barrier film that protects a 5 μm particle containing OLED. The OLED must have a lifetime of greater than 10 years at 25 °C and 50% relative humidity.

We present a detailed study of the permeation of water into barrier films made of SiO_2-silicone hybrid material that was deposited under a particular set of plasma conditions. To demonstrate a minimum of 10 years at 25 °C and 50% relative humidity, accelerated tests at 85 °C and 85% relative humidity are performed. 500 hours of storage at 85 °C and 85% relative humidity for bottom emitting OLEDs is targeted. We quantitatively translate the 500 hour lifetime to a lifetime at ambient conditions of 25 °C and 100% relative humidity, 30 °C and 100% relative humidity and extreme operating condition of 38 °C and 90% relative humidity. To achieve the aim, we have employed a four step strategy:

1. We introduce simple, particle insensitive techniques for evaluating the permeability of water in a barrier layer. Using these techniques, we identify the water permeation rate for barrier films deposited at different process conditions.
2. We study encapsulation of particles by introducing standard test particles on the substrate of the OLED. From the results, we propose a three layer barrier film deposited in a single process. Each layer has different water vapor transmission rate, mechanical stress and particle encapsulation capability.
3. We elucidate the importance of removing sideways permeation in barrier films.
4. We propose strategies to reliably predict OLED lifetime.

1.5 Barrier film development strategy

1.5.1 Barrier material characterization

To overcome the disadvantages of slow OLED lifetime testing to determine the barrier film quality, we have developed two sensitive, simple and rapid techniques for measuring the diffusion coefficient of water in a flexible barrier film. We predict the OLED lifetime from the results of these techniques. We measure the electrical capacitance of capacitors that use the barrier film as dielectric. Alternatively we extract the film's mechanical stress in barrier film/silicon wafer couples. Both electrical capacitance and mechanical film stress are highly sensitive and proportional to the amount of water dissolved in the barrier film. By monitoring the evolution of capacitance and film stress, the diffusion coefficient of water in the barrier film is measured. High temperatures and water vapor pressures (up to 200 °C and 1 atmosphere in our case) are employed to rapidly obtain the diffusion coefficient. For obtaining the permeability of water through the barrier film a measurement of the dissolved water concentration is also needed. One Secondary Ion Mass Spectrometry (SIMS) measurement will provide that.

1.5.2 Particle encapsulation

The presence of particles on the surface of the OLED break the continuity of the encapsulation. Our observations show that particle size range up to 5 μm. A barrier film must be twice as thick as the particle itself to achieve encapsulation. This increases the device fabrication time and cost. Efforts to reliably eliminate the presence of particles have been unsuccessful. The randomness in the size and shape of the particles have prevented a systematic study of their encapsulation.

We introduce a systematic study to encapsulate the OLED even in the presence of particles. A design based strategy was employed to encapsulate particles with a barrier thickness smaller than the size of the particles. We microfabricate standard test "particles", use glass fibers as intentional particles and perform barrier deposition on them. By varying the process conditions and observing the cross section of particles with encapsulation we identify a multilayer barrier film that in a single process encapsulates a particle of given size. The total thickness of the multilayer barrier is less than the size of the particle.

1.5.3 Reducing sideways permeation

Achieving 100% encapsulation on all devices is impossible because some particles are too big. As a result there are bound to be a fraction of devices with break in encapsulation. Such a break immediately shows up at high temperature and humidity (figure 1.4a). But given the randomness of the particle distribution on the surface of the device, the defect can appear away from the luminescent or pixel area. Such defects may feed water in to the OLED's luminescent area. But shrinkage of the luminescent area does not show up until prolonged tests in high temperature and humidity.

Delayed shrinkage because of sideways permeation dramatically reduces the reliability of lifetime prediction for the encapsulation. A detailed explanation of the direct relation between the reliability and sideways permeation is given in chapter 9. It is necessary to remove sideways permeation. We replace the traditional photoresist grid that is used to separate the cathode and the anode with an impermeable inorganic grid to reduce the sideways permeation.

1.6 Outline

We begin by addressing the existing barrier films used for OLED encapsulation and discuss their pros and cons. We analyze the prevalent techniques used to characterize barrier films.

Following that we explain our PECVD barrier deposition process. All the experimental work described in this thesis is based upon the barrier film fabricated with this process. The source gases, reactor design and baseline recipe are described.

It is followed by a review of the parameters that characterize permeation through a barrier film. Then we survey the mechanism of water diffusion into fused silica, as its material properties are closest to the material of our barrier. In successive steps, we introduce the necessary diffusion equations. A description of the experimental techniques follows: measuring a water concentration profile by SIMS, and measuring step-by-step, between exposures to water, the electrical capacitance or mechanical stress of the barrier film. The method of extracting water permeability using these techniques is explained. The PECVD process parameters that were employed during barrier film deposition on substrates of glass, metallized glass, or silicon wafers are listed. After that we describe the procedures used to expose film containing substrates to liquid H_2O, D_2O or H_2O^{18} or superheated H_2O steam. The subsequent three sections describe the experimental results, discuss them, and use them to predict the one-monolayer permeation time τ_{ML}, which is our measure of OLED lifetime.[2]

Then we describe a systematic study to understand the coating of particles by depositing the barrier films on standard particles made by silicon microfabrication, glass fibers and glass spheres. A cross section of the barrier film deposited over the microfabricated silicon particle and glass fibers is viewed in the SEM and the encapsulation is evaluated. The PECVD deposition power and the pressure is tuned and the encapsulation is evaluated. From the encapsulation study we design a

---

[2] 1 monolayer = 10^{15} molecules/cm^2 of water

three layer barrier film structure to encapsulate particles of 5 μm size. Glass spheres are used in testing encapsulation of barrier films deposited on OLEDs.

We change the deposition process power and pressure and evaluate water permeation and mechanical film stress. Along with this we use the information from the particle encapsulation study to encapsulate a Bottom Emitting Organic Light Emitting Diode, BOLED. We spread 5 μm glass bead spheres on the BOLED surface to act as intentional particles. We encapsulate the BOLED containing particles with a three layer 3.6 μm total thickness barrier film. We demonstrate an operating lifetime of 500 hours at 85 °C and 85% relative humidity even when these 5 μm size particles are present.

We explain how removing sideways permeation is necessary for obtain highly reliable lifetime predictions for OLEDs. In the final chapter we demonstrate an inorganic grid to reduce sideways permeation of water.

Chapter 2

Current barrier films and their evaluation

2.1 Existing barrier technology

Multiple barrier film designs have been brought up as options for making flexible displays. The films typically have alternating layers of impermeable films which has defects and permeable films that are conformal. Each inorganic/polymer pair is termed a *dyad*. The inorganic layers are prone to defects. The defects are either due to microdefects or due to break in encapsulation due to particles as described in the section 1.2. When multiple dyads are successively fabricated, the defects in alternating inorganic layers are randomly distributed. The random distribution of defects results in a long, tortuous path for water to permeate from the ambient atmosphere into the OLED. The mathematical description of the long diffusion path is given by Graff[14]. A few examples of multilayer barriers are described here.

Alternating layers of Al_2O_3 inorganic film and polyacrylate barriers have been shown to function as a flexible barrier film[5, 11, 28, 29, 30]. The inorganic layer is typically made of Al_2O_3 deposited by reactive sputtering at room temperature. The polymer layer is made of polyacrylate material deposited by flash evaporation of monomers. Post evaporation, the monomer is cured by exposure to UV radiation. The polymer layer is devoid of pin-holes and cracks but the bulk of the material has a high permeability for water. Typically 3-5 dyads or 6-10 layers are required for encapsulation.

Patent [31] describes the use of graded composition diffusion barrier to encapsulate OLEDs and substrates. Repeated pairs of SiO_xN_y/SiO_xC_y layers are deposited in succession through a plasma enhanced chemical vapor deposition process (PECVD). The SiO_xN_y is the inorganic layer with lower permeability but has defects. The SiO_xC_y is the polymer layer that separates the defects in the alternating SiO_xN_y layers. The principle of operation is same as the previous example. SiO_xN_y acts as the inorganic layer and SiO_xC_y behaves like a polymer layer.

Plasma Enhanced Chemical Vapor Deposited alternate SiO_x/SiN_x barriers have been demonstrated to perform as barrier films[32]. 6 stacks are used to meet OLED requirements.

2.1.1 Disadvantages of a multilayer structure

While the multilayer structure is effective in providing permeation protection at high dyad count, the structure has some disadvantages. 1. It takes a very long time to deposit the alternating inorganic/polymer structure due to the difference in the deposition equipment, increasing fabrication time and cost. 2. Special care needs to be taken care at the edges where the polyacrylate layer or the polymer layer is exposed. The polymer or polyacrylate layer has a high WVTR of 1-100 g/m^2/day. To prevent water from permeating through the edges, a wide bezel is required. Alternatively, the inorganic layers in successive deposition steps are increased in size to wrap the edges of the underlying polyacrylate layer. This again increases the deposition bezel of the device. 3. The thickness of the resultant structure and the rigidity of the inorganic Al_2O_3/SiN_x layer renders the barrier film prone to cracking upon bending preventing the barrier from being flexible.

2.1.2 Princeton hybrid barrier film

We have developed a flexible barrier film to package OLEDs. The barrier film, is deposited from the source gases hexamethyldisiloxane and oxygen in a PECVD. The resultant film is has low permeability yet stays flexible. The film is deposited in one run, unlike the typical multilayer structures which require multiple deposition chambers. During the deposition of the hybrid barrier film, the deposition recipe can be altered to tune the permeability to water, conformal coating nature, mechanical stress and rate of deposition. The deposition process is described in chapter 3.

2.2 Measurement techniques

The permeation rate of water can be measured by using commercially available tools such as Mocon and Technolox. The fundamental design of all these tools are similar and are based on standard ASTM F1249[33]. Two chambers are separated by the barrier film. One of the chambers is filled with a tracer material and the other side is emptied of all the tracer material. The tracer can be either water vapor or isotopic water or any gaseous molecule. As a function of time, the tracer molecules diffuse from one side to another. By using a detector that can quantitatively identify the small quantities of tracer in the empty chamber, the rate of diffusion can be measured.

Mocon Permatran test uses normal water as a tracer. One chamber is filled with water vapor, and in the adjoining chamber, the quantity of water is measured over time. Infrared absorption due to water vapors is monitored in the second chamber and is translated to water concentration. Technolox utilizes normal water as tracer and measures the rate of pressure increase in the second chamber. The increase in pressure is translated to water permeation.

Typical tests using two chambers do not measure water vapor transmission rates required by OLED of 10^{-6} g/m^2/day. High accuracy can be obtained by using a tritiated water source, HTO[34, 35]. One chamber is filled with tritiated water vapor, HTO. The dry side has a container of LiCl which absorbs the diffusing tritiated water. A scintillation counter measures the number of HTO molecules absorbed by LiCl. From the reading of the scintillation counter, the water permeation rate is measured. The handling and disposal of tritiated water is a tedious and involved process.

Calcium oxidation rate is a way to measure the permeating water quantity[26, 36, 37]. Evaporated calcium thin-films are oxidized rapidly upon exposure to water. The opaque calcium becomes transparent CaO and $Ca(OH)_2$ upon oxidation. The conductive calcium also becomes electrically resistive CaO and $Ca(OH)_2$ as it gets oxidized. By monitoring the optical transparency and/or electrical conductance, the water vapor transmission rate is measured. Calcium is typically evaporated on top flexible plastic substrate coated with barrier film. The other side of the calcium is sealed with a glass plate and UV edge sealants. Water permeates through the plastic substrate and through the barrier film and oxidizes the calcium.

The two chamber tests and the calcium tests measure the sum of water vapor transmission arising from both defects and from diffusion. The tests do not isolate the effects of diffusion alone. This results in uncertainty in measured barrier material properties as it is very difficult to identify the dominant water permeation mode. We have developed sensitive, accurate and quick measurements that can identify the intrinsic diffusion quantity of water in a material. The techniques measure the WVTR due to diffusion through the film even when defects are present in the film. Chapter 4 describes these techniques.

Chapter 3

Plasma deposition

The hybrid layer is deposited in a Plasma Enhanced Chemical Vapor Deposition (PECVD) system from hexamethyldisiloxane (HMDSO) vapors and oxygen on substrates that are nominally at room temperature. HMDSO comes as a non-toxic, non-explosive liquid whose structure and properties are given in figure 3.1 and table 3.1 respectively. It is liquid at room temperature, making it convenient for storage, and has a vapor pressure of 33 Torr at 25 °C[38].

HMDSO vapor without oxygen dilution is used as a source gas to fabricate plasma polymerized (pp)-HMDSO films. Extensive study of pp-HMDSO films have been performed by several research groups [39, 40, 41]. pp-HMDSO films have been used as corrosion protection layers, electrical insulators, humidity sensors and chemical barrier coatings. They are also used as scratch resistant coatings in optical lenses, optical filters[42, 43, 44, 45].

Detailed description of the deposition has been presented by Mandlik[24] and Han[46]. The HMDSO vapors are fed along with oxygen into an otherwise evacuated chamber. Applying a radio-frequency power between two electrodes creates a discharge in the gas mixture between the

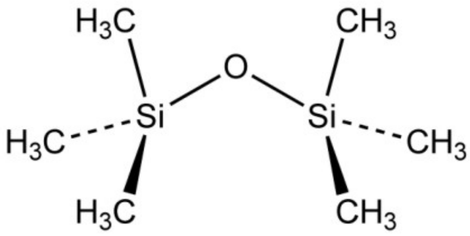

Figure 3.1: Molecular structure of hexamethyldisiloxane (HMDSO).

Table 3.1: Hexamethyldisiloxane properties

Molecular mass	162 g/mol
Boiling point	101 °C
Density at 20 °C	0.763 g/cm^3
Relative dielectric constant	2.17
Flash point	-1 °C
Heat of evaporation	7.2 kcal/mol
Refractive index	1.46

electrodes (plasma). Energetic electrons produced by the discharge split the HMDSO molecule into several pieces in a series of reactions (which are discussed in the next section). The oxygen in the plasma oxidizes the hydrogen and carbon. The resulting highly reactive radicals deposit when it comes in contact with a surface, to form a film. The film has a silicon and oxygen network with alkyl side chains and has the chemical composition $SiO_xC_yH_z$. The physical properties sit between silicone polymer and inorganic silicon dioxide. Hence it is termed a *hybrid*. The amount of Si-O-Si bonds and attached alkyl chains (-CH_3, -H) determine the hardness, elasticity and permeation properties[47, 48, 49, 50]. The properties can be controlled by tuning the deposition conditions: oxygen dilution, pressure, substrate temperature and plasma power [51, 52]. We use this to our advantage to deposit a hybrid layer that is devoid of pin-holes, as a polymer film would be, yet has the low bulk permeability of silicon dioxide.

3.1 Plasma process

Deposition of the hybrid from HMDSO and oxygen is a multi-step process that is heterogeneous because it proceeds partly in the gas phase and partly on the substrate surface. The HMDSO monomer fed into the chamber is split by electron impact. Dissociation of the monomer is thought to occur on the -CH_3 group[50]. The role of oxygen in the gas phase may be limited because slowly replacing the oxygen by argon does not change the concentration of intact HMDSO molecules in the exhaust from the plasma[24]. The Si-O bond energy is 8.3 eV, much higher than the C-H bond of 3.5 eV and the Si-C bond of 4.6 eV. Therefore the Si-O bond is preserved in the HMDSO activation process. The activated species, which largely are electrically neutral, diffuse in the gas phase until they hit a surface. If they collide with another activated species and make a bond with it, they may form the nucleus of a particle in the gas phase. The probability of forming a particle in the gas phase is determined by the pressure, flow rate, and the plasma power. If the activated species stick to a surface, they continue to be bombarded by molecules, radicals, and electrons. Water and carbon dioxide are released as byproducts from the surface. Most carbon atoms are oxidized by oxygen bombardment on the surface[53].

Oxygen plays a strong role in the hybrid formation. In plasma deposition from HMDSO and argon, nitrogen or helium, instead of oxygen, the carbon stays in the deposited film, which results in a pp-HMDSO like deposited layer. Deposition with oxygen produces silicon dioxide like layers[54].

3.2 Deposition setup

Figure 3.2 is a schematic of the deposition system at Princeton University. Liquid HMDSO is stored in a flask kept at 33 °C. The vapor pressure of HMDSO at that temperature is 70 Torr. The vapors are fed to the reactor through a 0.5-inch outer diameter stainless steel pipe. This pipe is heated with flexible fiber glass insulated heating tape to prevent condensation of HMDSO vapor inside the piping. The flow rate of HMDSO vapor is controlled by a MKS 1150C mass flow controller(MFC). The MFC can feed HMDSO at flow rates from 0.4 sccm to 10 sccm. The MFC is warmed up to 35 °C to prevent vapor condensation. The HMDSO is premixed with oxygen before the gases enter the plasma chamber. The nitrogen line serves both as an optional nitrogen source for deposition and as a vent gas source.

3.3 PECVD reactor design

Figure 3.3 is the cross section of the deposition zone of the reactor. Premixed HMDSO vapor and oxygen flow into the chamber bottom through a gas dispersion ring. The sample is mounted at the top facing down at the plasma. The deposition is from bottom to top. The sample is held in place by a copper substrate holder. The discharge is produced in a triode configuration. The grounded copper substrate holder forms the top electrode of the triode structure. The copper substrate is bolted to the lid of the reactor which can be removed to mount the samples. The lid closes the cylindrical reactor and is sealed with a viton O-ring. The middle powered electrode of the triode

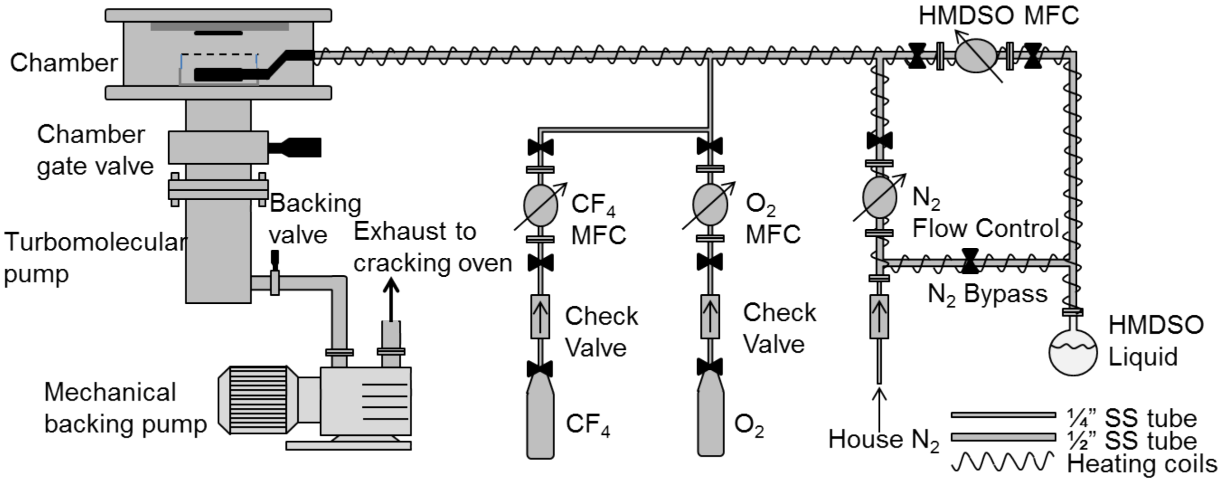

Figure 3.2: Schematic of the Single Chamber Plasma Enhanced Chemical Vapor Deposition(PECVD) system at Princeton University.

is 6 inches in diameter and is made out of a 0.03 inch thick perforated stainless steel plate. The perforation makes 23% of open space in the plate. The perforation allows the active species in the plasma region between the middle and the bottom electrode to diffuse towards the top electrode holding the sample. The gas dispersion ring is grounded and forms the bottom electrode. The middle electrode is the powered electrode and is connected to a radio frequency (RF) power supply operating at 13.56 MHz through a matching network. The middle electrode is held in place by a glass spacer cylinder of 6 inch diameter. The distance between the top and the middle electrodes is adjusted from 0.7 to 1.1 inches and the distance between middle and the bottom from 0.8 to 1.2 inches. A standard barrier is deposited in a configuration with top and middle electrode separation of 1.1 inches and middle and bottom electrode separation of 0.8 inches. The middle electrode, gas dispersion ring and the glass cylinder spacer can be removed for cleaning when necessary. The copper substrates are of two kinds. One is a water cooled solid copper block. The second is a copper plate with resistance heaters and thermocouples for deposition at temperatures up to 150 °C.

3.4 PECVD Deposition

A standard material is deposited with mass flow rates of 1.1 sccm of vapor HMDSO, 33 sccm of O_2, at a chamber pressure of 110 mTorr, radio frequency deposition power of 70 W and with the

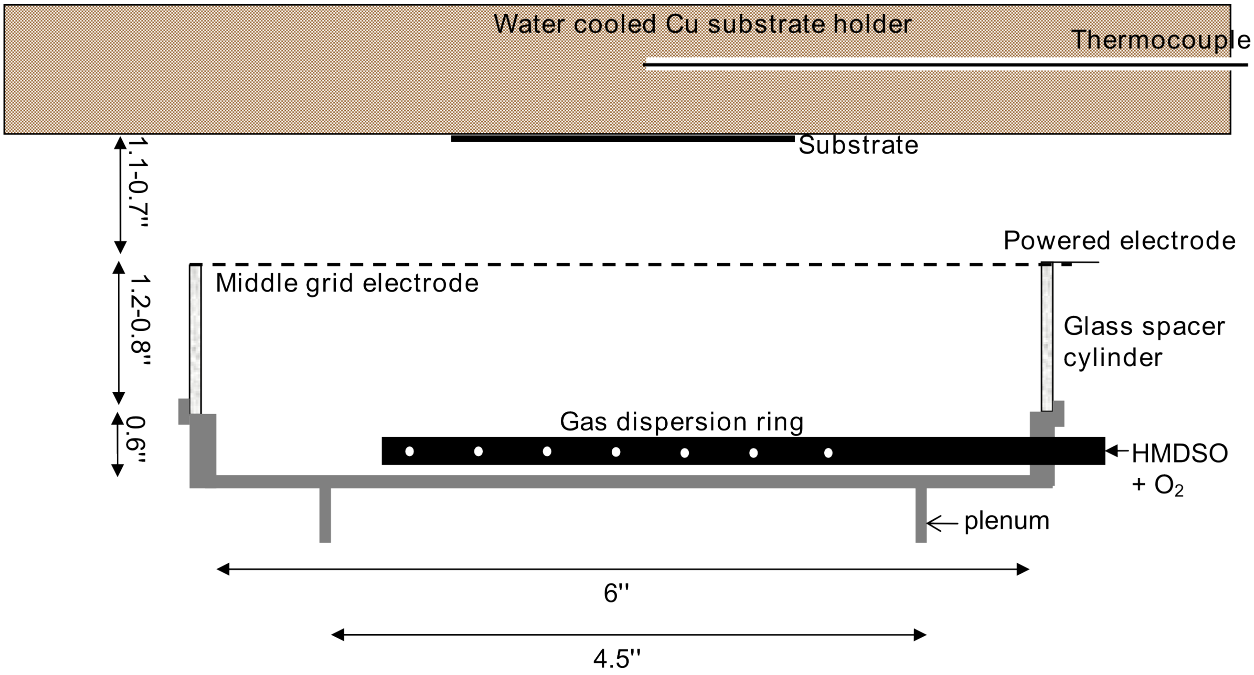

Figure 3.3: PECVD electrode configuration.

Table 3.2: Typical deposition conditions of a hybrid barrier film.

Parameter	Value
HMDSO	1.1 sccm
O_2	33 sccm
Pressure	110 mTorr
Power	70 W
Growth rate	0.9 μm/hour

substrate holder at nominal room temperature.[1] Table 3.2 lists the deposition recipe parameters of a typical film. The barrier film is silicon dioxide like in composition with a small residual carbon content. A detailed study of PECVD deposition rate, wet and dry etch rates, infrared absorption spectra, water droplet contact angle, surface roughness, atomic force microscopy phase shift, coefficient of thermal expansion, critical tensile strain, elastic modulus, indentation hardness, optical absorption spectrum, refractive indices, relative dielectric constants, and electrical conduction has been published[16].

---

[1] Exact film properties are tuned on application requirements such as water permeability, conformable coating of surface profiles and of incidental particles, desired radius of curvature during bending and rolling, film stress and film stress compensation.

Chapter 4

Measurement of barrier diffusion properties

4.1 Permeation barrier film properties and requirements

The barrier film quality is captured in two properties, the steady-state permeability P and the water vapor transmission rate WVTR. Each of these properties is evaluated at a specified temperature and relative humidity. P is stated in units of g/cm.s, and WVTR in g/m^{2}day. In a barrier free of defects, P is the product of the diffusion coefficient D and the solubility S of water at a given temperature and relative humidity. The solubility S of the water is also the dissolved water concentration at the exposed barrier surface, n_0. While the cgs unit of g/cm^3 is commonly employed for solubility when calculating P, we will use the solid-state electronics unit of molecules/cm^3 because our targeted result is τ_{ML}, the permeation time for one monolayer of water molecules to reach the cathode. The normalized solubility S_n, expressed in g/cm^{3}atm, is the concentration of water in the barrier at the ambient water vapor pressure of $p_{H_2O} = 1$ atm, at a specified temperature T. Below $T = 100$ °C the normalized solubility S_n is calculated from measurements at the saturation vapor pressure of water $p_{H_2O} < 1$ atm. The solubility S is assumed to be proportional to p_{H_2O} following Henry's law. The permeation rate WVTR is the diffusive flux of water through the barrier when its concentration gradient is uniform. WVTR is calculated by dividing the permeability P at the given temperature and humidity by the thickness h of the barrier, $P/h = DS/h$. A widely quoted requirement for the

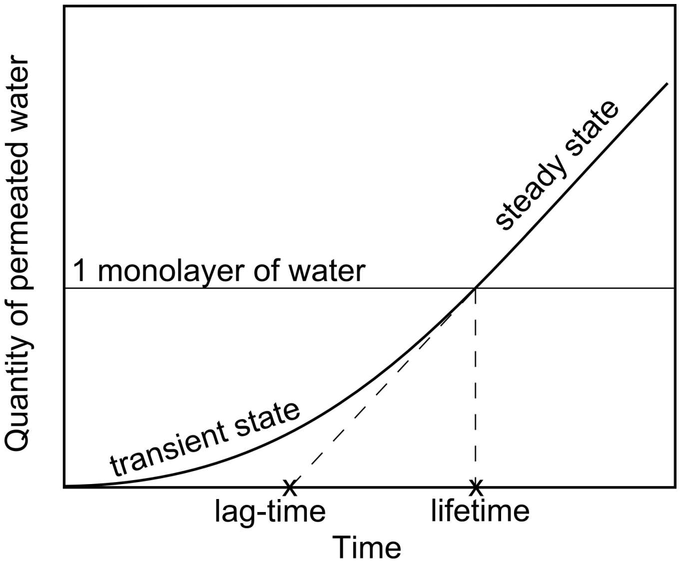

Figure 4.1: The time taken for 1 monolayer of water to permeate and reach the OLED is defined as the "lifetime", τ_{ML}. The time taken for permeation rate to reach steady state is the "lag-time" [14].

allowable WVTR of water into OLEDs is 10^{-6} g/m^2/day at room temperature. The equivalent requirement for the oxygen transmission rate (OTR) ranges from 10^{-5} to 10^{-3} cm^3/m^{2}day[5, 19].

A barrier's life begins in as-deposited condition with zero extraneous water and eventually reaches steady-state when it transmits water at a constant rate, the WVTR. The time until steady-state is reached is called the "lag-time"[14]. Currently there are no established methods to exactly measure the failure quantity of water. One criterion employed for highly effective permeation barriers is that the lag-time be comparable or even longer than the required OLED lifetime. However, defining the barrier lifetime as the lag-time derived from its WVTR may lead to inaccurate lifetime estimates. To set a precise value for the failure time, we use the time by which one monolayer of water has permeated through the barrier, τ_{ML} as the criterion as shown in figure 4.1. τ_{ML} is the *lifetime* or *fail time.* Our target for the single-layer permeation barrier film is a τ_{ML} longer than 10 years. Permeation of one monolayer of water over 10 years corresponds to a WVTR of 8.2×10^{-8} g/m^2/day under steady state. The symbols and the units discussed henceforth are listed in table 4.1.

Table 4.1: Symbols and units

	Symbol	Units
Diffusion coefficient	D	cm^2/s
Solubility & Concentration in the surface	S or n_0	$molecules/cm^3$
Concentration	$n(x, t)$	$molecules/cm^3$
Film thickness	h	nm
Time	t	seconds or hours or years
Total dissolved water at time t in the film	$N(t)$	$molecules/cm^2$
Saturated total dissolved water at time $t = \infty$	$N(\infty)$	$molecules/cm^2$
WVTR	WVTR	g/m^2day
Property such as capacitance or stress that is proportional to solubility of water	Π	depends on specific property
Depth into the layer, from the surface	x	cm
Dry barrier dielectric constant	ε_0	No unit
Barrier dielectric constant	$\varepsilon(x, t)$	No unit
Dielectric constant calibration factor	K_ε	$1/(molecules/cm^3)$
Capacitance at time t	$C(t)$	pF
Saturated capacitance	$C(\infty)$	pF
Area of the capacitor	A	cm^2
Surface stress	$\gamma(t)$	MPa.cm
Average film stress	$\sigma(t)$	MPa
Stress calibration factor	K_σ	$MPa/(molecules/cm^3)$
1 monolayer permeation time	τ_{ML}	seconds or hours or years

4.2 Analysis of diffusion and application to film properties that depend on water content

When a hybrid film is exposed to water, the film's electrical capacitance and mechanical stress increase over time. Both observations suggest that water diffuses into the film and changes its physical properties. The capacitance rises because the dielectric constant of H_2O is far higher than that of SiO_2. The film stress rises because H_2O causes the film to swell. The film however is constrained by its adhesion to the substrate, resulting in a stress build up. Fick's law of diffusion describes the diffusion of water into the film. Given its large surface area to thickness ratio, the film can be treated as an one-dimensional system with diffusion proceeding from $x = 0$ at the film's surface to $x = h$ at the bottom surface of the film. The accumulation of water molecules in a given location, $n(x,t)$ and the water flux $J(x,t)$ at depth x in the barrier film is given by:

$$\frac{dn(x,t)}{dt} = D\frac{d^2n(x,t)}{dx^2} \tag{4.1}$$

$$J(x,t) = -D\frac{dn(x,t)}{dt} \tag{4.2}$$

Here $n(x,t)$ is the concentration of dissolved water molecules, t is the time, D is the diffusion coefficient at depth x from the surface of the barrier, and J is the flux of water molecules at x. We will see that all diffusion data that we measured conform to solutions of Fick's laws, leading to an erfc profile in our case (with the exception of the O^{18} concentration profile in the H_2O^{18} soak tests).

The concentration of water molecules in the surface of the barrier film at $x = 0$, n_0, is equal to the solubility of water S at the test temperature and humidity. When n_0 of a semi-infinite sample ($\sqrt{Dt} << h$) is constant, the concentration profile at time t is given by the complementary error function[1]:

$$n(x,t) = n_0 \times \text{erfc}\left(\frac{x}{2\sqrt{Dt}}\right) \tag{4.3}$$

---

[1] OLEDs are *de facto* infinite sinks for water. The chromium-on-glass slide or silicon wafer substrates described later in this chapter are treated as impermeable substrates

When $\sqrt{Dt} << h$, the diffusion coefficient D can be extracted by fitting the complementary error function of equation 4.3 to a measured concentration profile. Deuterated and tritiated water[55] have been used as markers to determine the water diffusion coefficient and the solubility in silica glass in this manner.

4.2.1 Film deposited on an OLED

Two boundary conditions apply to a barrier film of thickness h on an OLED:

1. The top surface (at $x = 0$) has a constant water concentration of n_0 that is set by the test temperature and relative humidity.
2. The OLED acts as a perfect sink for water. The concentration at the interface to the OLED (at $x = h$) is zero.

Solving equation 4.1 for these boundary conditions results in the total number of water molecules that has permeated into the OLED per unit surface area at time t, $Q(t)$, as given by Crank[2]:

$$Q(t) = \frac{Dtn_0}{h} - \frac{hn_0}{6} - \frac{2hn_0}{\pi^2} \sum_{m=1}^{\infty} \frac{(-1)^m}{m^2} e^{-Dm^2\pi^2 t/h^2} \tag{4.4}$$

For long durations, equation 4.4 approximates as[14]:

$$Q(t) = \frac{Dn_0}{h} \left(t - \frac{h^2}{6D} \right) \tag{4.5}$$

The WVTR and the lag time are hence expressed as:

$$\text{WVTR} = \frac{Dn_0}{h} \tag{4.6}$$

$$\text{Lag time} = \frac{h^2}{6D} \tag{4.7}$$

4.2.2 Film deposited on an impermeable substrate

The diffusion begins the same as in the OLED case but eventually the film saturates with water through its entire thickness. Then the film contains $N(\infty) = n_0 \times h$ molecules of water per unit

---

[2] Equation 4.24 in Crank, reference [56].

surface area. At time t the number of water molecules absorbed by the permeation barrier, $N(t)$, as given by Crank[3]:

$$\frac{N(t)}{N(\infty)} = 1 - \sum_{m=0}^{\infty} \frac{8}{(2m+1)^2\pi^2} e^{-D(2m+1)^2\pi^2 t/4h^2} \tag{4.8}$$

For short durations, when $\sqrt{Dt} << h$, the expression can be approximated as

$$N(t)^2 = 4\left(\frac{N(\infty)}{h}\right)^2 \left(\frac{Dt}{\pi}\right) \tag{4.9}$$

hence D is given by

$$D = \left(\frac{h^2\pi}{4N(\infty)^2}\right)\left(\frac{N(t)^2}{t}\right) \tag{4.10}$$

Before the permeation barrier saturates with water, in other words when $\sqrt{Dt} < h$, the diffusion coefficient D can be extracted measuring the total amount of dissolved water at time t, $N(t) = \int n(x,t)dx$ and the saturation quantity of dissolved water, $N(\infty)$. The diffusion coefficient is obtained from equations 4.9 and 4.10. Equation 4.9 can also be employed to measure D in semi-infinite barriers if the surface concentration n_0 is known. In this case equation 4.9 changes to:

$$N(t)^2 = 4n_0^2\left(\frac{Dt}{\pi}\right) \tag{4.11}$$

The weight of absorbed water is extremely small. For example when a 1 µm thick barrier absorbs water at a concentration of 1% by weight, the barrier weight will increase by 2.66 µg/cm^2. Some chemical, electrical and mechanical properties undergo substantial changes when water diffuses in. We identify a property Π that changes as a function of the total quantity of dissolved water $N(t)$. Π can be used to determine the diffusion coefficient. The inspection of equation 4.10 shows that the D can be extracted from measurements of any property that is proportional to N. By selecting the property that changes the most, the diffusion coefficient can be measured with high sensitivity. In our experiments Π stands for a function of electrical capacitance C or mechanical film stress σ. When Π changes proportionally to $N(t)$ such that $(\Pi(t) - \Pi(0)) \propto N(t)$, equation 4.9 can be

---

[3] Equation 4.18 in Crank, reference [56].

rewritten as:

$$(\Pi(t) - \Pi(0))^2 = 4 \left(\frac{\Pi(\infty) - \Pi(0)}{h} \right)^2 \left(\frac{Dt}{\pi} \right) \tag{4.12}$$

Therefore by measuring the *change* in chemical, electrical or mechanical property Π at a fixed temperature and humidity, the diffusion coefficient D can be evaluated. The thermal activation energy of the diffusion coefficient E_D can be calculated from diffusion coefficients D measured over a range of temperatures.

The thermal activation energies for S and $N(\infty)$ are stated for a fixed water vapor pressure p_0. The small concentrations of water in the barrier of less than 1 mol percent justify two assumptions: the property $\Pi(t)$ varies linearly with the quantity of dissolved water molecules $N(t)$; and the proportionality constant relating them is temperature independent. Then the thermal activation energy for the solubility of water E_S can be determined from $N(t = \infty, T)$. $N(t = \infty, T, p_{H_2O})$ is measured as a function of temperature and vapor pressure and then normalized to a fixed water vapor pressure p_0 using $N(t = \infty, T) = N(t = \infty, T, p_{H_2O}) \times (p_0/p_{H_2O})$.

We assume that the concentrations of water established by exposure over the temperature range of our experiments, 65 °C to 200 °C, do not change when the samples are brought to room temperature and then are evaluated in ambient atmosphere, or in vacuum as in the case of SIMS.

4.3 Experimental techniques to measure water concentration and diffusion

We perform secondary ion mass spectrometry combined with sputter profiling and measure electrical capacitance and mechanical stress to find out solubility and diffusion coefficient of water in the barrier. The films are deposited with the recipe described in table 3.2. While the sample structure was adapted to the respective evaluation technique, all samples were exposed to water in the same way. The setup is described in appendix A. The temperature determines the rate at which the water diffuses and in turn the rate of change of electrical capacitance and film stress. Temperature and humidity together determine the solubility of water S or surface water concentration n_0 in the barrier.

4.3.1 Secondary Ion Mass Spectrometry

Two samples are evaluated by SIMS. One is held in boiling heavy water and the other in boiling H_2O^{18}. The film, after testing is far from steady state to ensure $\sqrt{Dt} << h$. Then the samples can be assumed to be semi-infinite and the concentration of water follows a complementary error function distribution with diffusion coefficient D given by equation 4.3. The samples have a background concentration of hydrogen that arises from the PECVD deposition. This background concentration is comparable to the maximum concentration of hydrogen from in-diffusing water and is about 10,000 ppm. To distinguish between the as-deposited and in-diffusing hydrogen we expose the SIMS samples to heavy water, D_2O, and evaluate the concentration profiles of both hydrogen and deuterium. Because the as deposited hydrogen concentration of the layer is 10,000 ppm, the natural abundance of its (as-deposited) D of 150 ppm does not interfere with the SIMS measurement.

The other SIMS sample is exposed to H_2O^{18} to distinguish between hydrogen and oxygen diffusion and to identify the mechanism of water permeation. Because the natural isotopic abundance of O^{18} is 2040 ppm, the as deposited concentration of O^{18} in the layer with a composition close to SiO_2 is comparable to the concentration that diffuses in.

4.3.2 Electrical Capacitance

The as-deposited permeation barrier material has a dielectric constant of $\epsilon_0 = 3.9$, the same as SiO_2[16]. Because water molecules are highly polarizable, they can raise the dielectric constant of the barrier material considerably even when dissolved in small quantities. In capacitors made with the barrier as the dielectric (Figure 4.2), the capacitance rises upon exposure to water. As in humidity sensors made with dielectric of organic polymers[57], the capacitance rises linearly with rising partial pressure of water. In our case, the highest concentration that water reaches is small, in the order of 1 atomic percent. The dielectric constant $\epsilon(x,t)$ of a homogeneous mixture of a host with dielectric constant ϵ_0 with a solute concentration $n(x,t)$ is given by Landau[58]:

$$\epsilon(x,t) = \epsilon \left(1 + K_\epsilon \times n(x,t)\right) \tag{4.13}$$

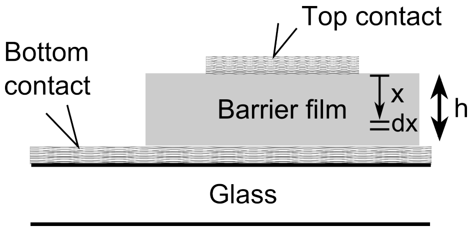

Figure 4.2: Schematic cross section of capacitors with the barrier material as dielectric. The capacitance change upon exposure to water is monitored to extract the diffusion coefficient D. The top contact is made of a thin porous chromium film.

Simple linear expressions of this form are also valid for *in*homogeneous mixtures that contain small quantities of a second phase[59].

To understand how the water diffusion affects the capacitance of the structure, let us analyze a capacitor of thickness h given by figure 4.2. An infinitesimally thin slab of thickness dx at a depth of x contains a small concentration $n(x,t)$ of molecularly dissolved water at time t. The local dielectric constant is given by equation 4.13. For a capacitor of area A and thickness h, the capacitance at time t is then given by:

$$\frac{1}{C(t)} = \int_0^h \frac{dx}{A\epsilon_0(1 + K_\epsilon n(x,t))} \tag{4.14}$$

For a given temperature T and water vapor pressure p_{H_2O}, the surface concentration of water stays constant at $n_0 = n_0(T, p_{H_2O})$ throughout the experiment. The thickness of the capacitor, h, is assumed to be constant as it is minimally raised by swelling. The concentration of water in the dielectric $n(x,t)$ at depth x and time t is given by the complementary error function distribution given in equation 4.3. If we assume that the change in dielectric constant is small because water uptake is small, then equation 4.14 can be re-written as a Taylor expansion around $K_\epsilon n_0 = 0$. The second order and higher terms are ignored to get:

$$\frac{1}{C(t)} = \int_0^h \frac{dx}{A\epsilon_0} \left(1 - K_\epsilon n_0 \mathrm{erfc}\left(\frac{x}{2\sqrt{Dt}}\right)\right) dx \tag{4.15}$$

Since the diffusion profile is far from steady state, $\sqrt{Dt} << h$, the upper limit of the integral is extended to ∞ and we find that the square of the change of inverse capacitance is linear with time:

$$\left(\frac{1}{C(0)} - \frac{1}{C(\infty)}\right)^2 = \left(\frac{K_\epsilon n_0}{hC(0)}\right)^2 \times \frac{4D}{\pi} \times t \tag{4.16}$$

At time $t = \infty$ the capacitor is saturated with water, $n(x,t) = n_0$. Rewriting equation 4.14 at time $t = \infty$ we can show:

$$K_\epsilon n_0 = \frac{C(\infty) - C(0)}{C(0)} \tag{4.17}$$

Eliminating the unknowns in equation 4.16 results in:

$$\left(\frac{1}{C(0)} - \frac{1}{C(\infty)}\right)^2 = \left(\frac{C(\infty) - C(0)}{C(0)^2}\right)^2 \times \frac{4D}{h^2\pi} \times t \tag{4.18}$$

Thus from measurements of the initial capacitance $C(0)$, the capacitance $C(t)$ at time t of water exposure, and the saturated capacitance $C(\infty)$ the diffusion coefficient D can be evaluated. Equation 4.18 can be used to determine the diffusion coefficient of water in the barrier as long as the concentration of water $n(x,t)$ is small and the diffusion coefficient is independent of concentration, $n(x,t)$. The constant K_ϵ is calibrated against solubility, n_0, obtained through secondary ion mass spectrometry using equation 4.13.

4.3.3 Mechanical stress

As the water permeates a barrier, the barrier film tends to swell. When the barrier is bonded on a silicon wafer, lateral swelling is restricted by the substrate wafer. This results in the build up of a surface stress, γ in the barrier film. The change in surface stress is the property that is proportional to the quantity of dissolved water $N(t)$.

$$\gamma(t) - \gamma(0) = K_\sigma N(t) \tag{4.19}$$

For a barrier of thickness h and surface concentration n_0, upon saturation the surface stress becomes:

$$\begin{aligned} \gamma(\infty) - \gamma(0) &= K_\sigma \times N(\infty) \\ &= K_\sigma \times n_0 \times h \end{aligned} \tag{4.20}$$

For a barrier, the average stress $\sigma(t) - \sigma(0) = (\gamma(t) - \gamma(0))/h$ is surface stress per unit thickness of the barrier. Hence saturated average stress is given by $\sigma(\infty) - \sigma(0) = K_\sigma \times n_0$. The silicon wafer bends in response to the swelling barrier. From the change in radius of curvature of bending, the change in stress $(\sigma(t) - \sigma(0))$ at time t is calculated using the Stoney[60] equation given below. $R(t)$ is the change in radius of barrier containing silicon wafer at time t with respect to the bare silicon wafer. $R(0)$ and $\sigma(0)$ are the as deposited barrier on silicon wafer radius of curvature and mechanical stress respectively at time $t = 0$. E_w and h_w are the silicon wafer elastic constant and thickness respectively.

$$\sigma(t) - \sigma(0) = \frac{E_w}{6R(t)} \frac{h_w^2}{h} - \frac{E_w}{6R(0)} \frac{h_w^2}{h} \tag{4.21}$$

The change in stress is linear with the water uptake $N(t)$. Hence $(\Pi(\infty) - \Pi(0))$ of equation 4.12 is replaced with change in average stress $(\sigma(\infty) - \sigma(0))$ to obtain:

$$(\sigma(t) - \sigma(0))^2 = 4 \left(\frac{\sigma(\infty) - \sigma(0)}{h} \right)^2 \left(\frac{Dt}{\pi} \right) \tag{4.22}$$

From measuring the change in average stress of the barrier and its saturation value, the diffusion coefficient of water can be found.

The thermal activation energy of the diffusion is calculated by measuring the diffusion coefficient of water over a range of temperatures. The solubility or the surface concentration is proportional to the saturated average stress. The thermal activation energy of solubility is measured from dependence on temperature of the saturated average stress $(\sigma(\infty) - \sigma(0))/p_{H_2O}$ normalized to 1 atmosphere water vapor pressure.

4.4 Experimental procedures

The SIMS and electrical capacitance samples were held in boiling water i.e., 100 °C and 100% relative humidity. For stress measurement, the samples were exposed to temperatures ranging from 65 °C to 200 °C to obtain temperature dependences of diffusion coefficient and solubility. For temperatures below 100 °C, the samples were immersed in water. For temperatures above 100 °C, the samples were placed on a temperature controlled hot plate. An inverted funnel is placed over the sample. A boiler generates steam which is fed into the stem of the funnel and on the way is super-heated to the same temperature as the hot plate. The vapor pressure remains at 1 atmosphere because the funnel rests loosely on the hot plate. For time series of stress measurements, the samples were taken off the hot plate and cooled down to the fixed room temperature of 22 °C before measurement. Appendix A describes this setup in detail.

4.4.1 SIMS measurement

To measure solubility and determine the diffusion coefficient by SIMS 660 nm barrier films were deposited on 100 mm diameter, 500 μm thick, <100> oriented silicon substrates. One wafer was exposed to heavy water and another to H_2O^{18}. The hydrogen and deuterium concentrations were calibrated against ion implanted thermally grown silicon dioxide samples. The samples were held in a boiling deuterium oxide bath at 101 °C for 12 hours and in boiling H_2O^{18} for 4 hours. The bath is fitted with a reflux condenser that traps any escaping deuterium oxide or H_2O^{18} steam. The sputter profile area for the SIMS experiments was 125 μm$\times$ 125 μm.

The raw ^{18}O data from SIMS is obtained in the form of counts. Natural oxygen 18 abundance is 0.2 atomic percent. Therefore the expected natural oxygen 18 concentration in SiO_2 is 9×10^{19} atoms/cm^3. The background oxygen 18 concentration measured in counts is calibrated with the known natural oxygen 18 atomic concentration in silicon dioxide.

4.4.2 Electrical capacitance

The capacitors were fabricated by sputter depositing a 100 nm chromium bottom contact on a glass substrate. A 200 nm blanket permeation barrier layer is deposited over this bottom electrode following which a thin 15 nm top chromium contact was deposited with a shadow mask. The top chromium contact is porous and does not slow down the diffusion of water into the capacitor structure. The top contact has an area of 0.79×10^{-2} cm^2. Shadow masking was used specifically instead of photolithography to prevent any exposure of the sample to solvents while at elevated temperatures during lithography when diffusing-in solvents and water may alter the dielectric constant of the barrier before the actual diffusion. The capacitors were held in boiling water i.e., 100 °C and 100% relative humidity. The capacitance was measured at 1 MHz with an Agilent 4275A LCR meter after taking the capacitor out of the boiling water and thoroughly blow drying it with nitrogen. The measurement is repeated at time intervals.

4.4.3 Mechanical stress

To measure the diffusion properties by monitoring mechanical stress, 1.5 μm thick permeation barrier layers are deposited on <100> oriented, 525 μm thick silicon wafers. The curvature of the wafer is measured before and after the deposition and after different time intervals during the diffusion experiment using a KLA Tencor P-15 profilometer. The thickness h of the barrier on the silicon dioxide is measured using a Nanospec reflectometer. From the bending radius of curvature, the stress of the barrier film is calculated from equation 4.21. The as-deposited film is compressive. The initial curvature change of the wafers, caused by layer deposition is first measured by profiling the wafer before and after deposition. The initial stress of the wafer is calculated. The stress change in the wafer upon water diffusion is calculated by subtracting the total stress in the wafer from the initial stress.

The accelerated test condition is varied from 65 °C to 200 °C while keeping the entire experimental setup at 1 atmosphere total pressure. For temperatures below 100 °C the barrier on silicon wafer was immersed in a constant temperature water bath. This is the equivalent of exposing the barrier to 100% relative humidity vapor at the experimental temperature. The description of the setup is given in appendix A.

To extract the diffusion coefficient, the saturated stress of the wafer, $\sigma(\infty)$, also needs to be measured. This measurement is quick at high temperatures as water diffuses to saturate the entire barrier thickness of 1.5 μm with water in a reasonable time period. Therefore, for temperatures $\geq$ 150 150 °C, the entire 1.5 μm barrier is saturated with water to measure the saturated average stress $\sigma(\infty)$. The saturation is reached when the stress no longer changes with exposure time. But at lower temperatures, saturating a 1.5 µm thick barrier with water can take months. To overcome this disadvantage, a thinner 100 nm barrier film on silicon wafer is tested. This thinner barrier film was saturated within days for measurement of the saturated average stress $\sigma(\infty)$ at temperatures less than 150 °C.

4.5 Results

4.5.1 SIMS measurement

The hydrogen and deuterium profile from SIMS analysis given in figure 4.3 is obtained after treatment in 101 °C boiling deuterium oxide for 12 hours. The deuterium profile is fitted with a complementary error function. Deuterium diffuses in with a diffusion coefficient of 4.2×10^{-15} cm^2/sec and a surface concentration of 7×10^{20} atoms/cm^3. An as-deposited sample has a hydrogen concentration of 6.5×10^{20} atoms/cm^3. The hydrogen diffuses out of the barrier with the same diffusion coefficient of 4.2×10^{-15} cm^2/sec. The surface concentration of hydrogen is 2.5×10^{20} atoms/cm^3. The sum of hydrogen and deuterium concentrations which corresponds to the excess water that is diffusing has also the same diffusion coefficient of 4.2×10^{-15} cm^2/sec. By subtracting the background hydrogen concentration of the barrier from the hydrogen+deuterium profile, the excess hydrogen+deuterium profile that has diffused in over time is obtained. The excess hydrogen + deuterium has a surface concentration of 3.2×10^{20} atoms/cm^3, which corresponds to a water molecular concentration in the surface of 1.6×10^{20} molecules/cm^3 or 5 mg/cm^3. The carbon concentration was measured in the sample along with hydrogen and deuterium. The concentration was constant as a function of depth with a value of 3×10^{20} atoms/cm^3.

The barrier film from a second deposition run after a 4 hour soak in boiling H_2O^{18} is subject to SIMS to obtain concentration profiles of hydrogen and oxygen-18. Figure 4.4 gives the excess concentration of H and O^{18} and their erfc and exponential fit, respectively. The hydrogen follows a complementary error function with an excess surface concentration of 2×10^{20} atoms/cm^3 and a diffusion coefficient of 3.5×10^{-15} cm^2/sec. The background concentration of hydrogen is 8.8×10^{20} atoms/cm^3. The hydrogen diffusion profile is comparable to the SIMS profile obtained with deuterium oxide diffusion experiment. Then O^{18} has a surface concentration of 1.8×10^{21} atoms/cm^3. A good exponential fit is observed after a depth of 20 nm into the barrier. The O^{18} fits

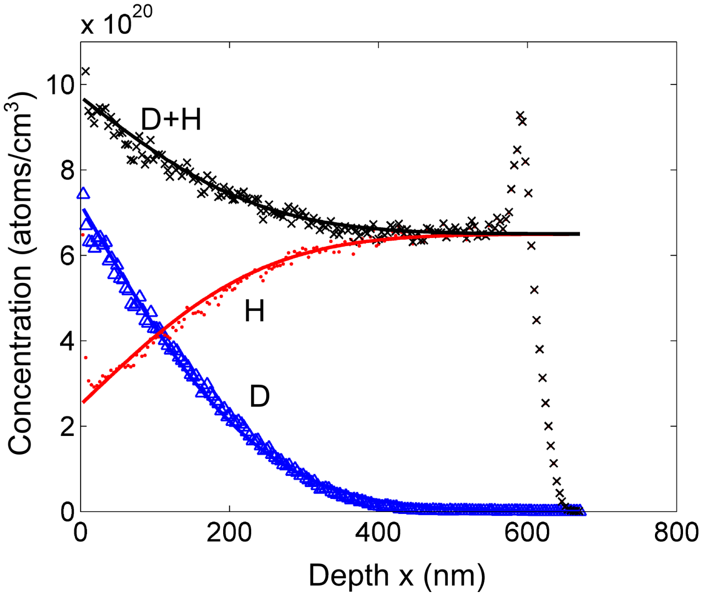

Figure 4.3: Hydrogen, deuterium and hydrogen+deuterium profiles measured in a 660 nm thick barrier on silicon a wafer after exposure to 101 °C boiling D_2O for 12 hours. All solid lines are complementary error function fits with a D value of 4.2×10^{-15} cm^2/sec. Table 4.2 gives the list the measured concentrations and diffusion coefficients.

Table 4.2: Summary of results inferred from SIMS profiling of the barrier after 12 hours of boiling in D_2O

Atoms/ Molecules	Diffusion Coefficient cm^2/s	Surface Concentration $atoms/cm^3$	Background $atoms/cm^3$	Profile
Hydrogen	4.2×10^{-15}	2.5×10^{20}	6.5×10^{20}	erfc
Deuterium	4.2×10^{-15}	7.2×10^{20}	$< 1 \times 10^{18}$	erfc
Hydrogen+ Deuterium	4.2×10^{-15}	9.7×10^{20}	6.5×10^{20}	erfc
Excess water (includes all isotopes)	4.2×10^{-15}	1.6×10^{20} $molecules/cm^3$ 5×10^{-3} g/cm^3	0	erfc
Carbon	0	3×10^{20}	3×10^{20}	constant

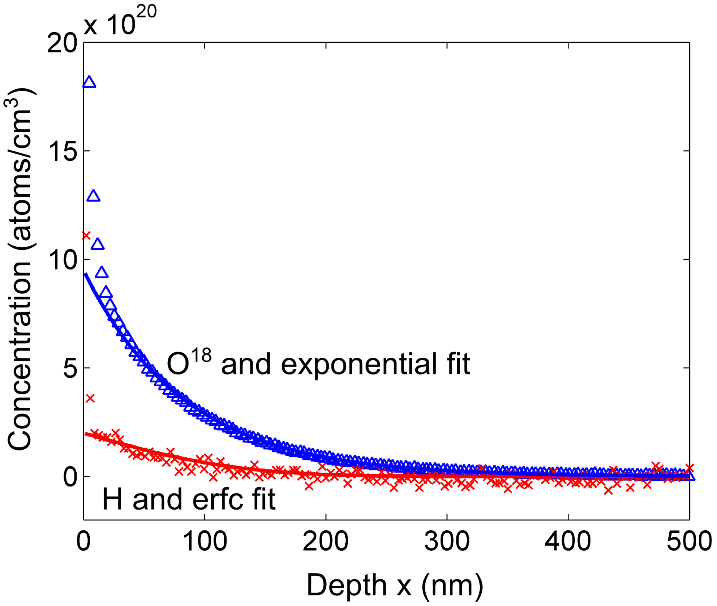

Figure 4.4: Excess hydrogen and oxygen 18 concentration profiles over the background. The hydrogen fits to a erfc function with a surface concentration of 2×10^{20} atoms/cm^3 and diffusion coefficient of 3.5×10^{-15} cm^2/sec. The excess oxygen 18 fits to an exponential fit $e^{(-x/L)}$ with a surface concentration 9.5×10^{20} atoms/cm^3 and a characteristic length L of 84 nm.

Table 4.3: Summary of results inferred from SIMS profiling after 4 hours in boiling H_2O^{18}

Atoms/Molecules	Diffusion Coefficient cm^2/s	Surface Concentration atoms/cm^3	Background atoms/cm^3	Profile
Oxygen 18	-	1.8×10^{21}	9×10^{19}	exponential profile with a characteristic length of 84 nm
Hydrogen	3.5×10^{-15}	10.8×10^{20}	8.8×10^{20}	
Excess O^{18}	-	9.5×10^{20}	0	
Excess hydrogen	3.5×10^{-15}	2×10^{20} molecules/cm^3	0	erfc

to an exponential fit $e^{(-x/L)}$ where L is the characteristic length of the profile. The characteristic length for the exponential fit is 84 nm. Table 4.3 summarizes the results obtained from the H_2O^{18} diffusion.

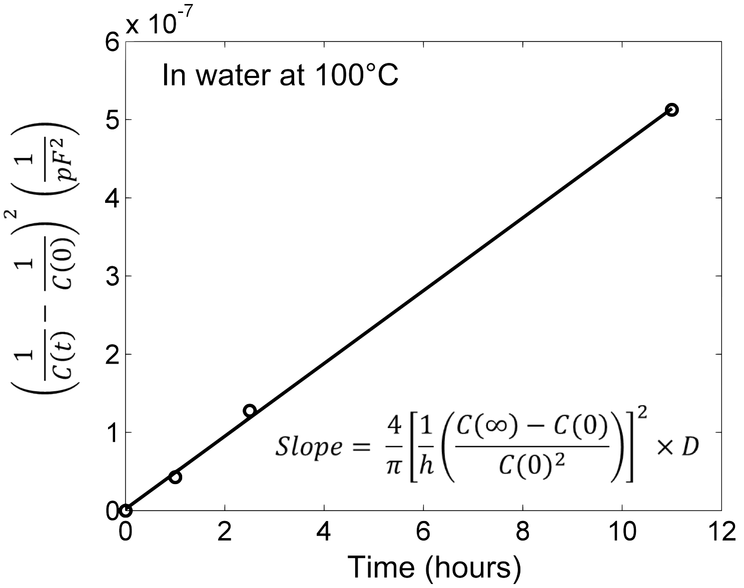

Figure 4.5: Square of the change in inverse capacitance vs time. The diffusion coefficient is 5.6×10^{-15} cm^2/sec.

4.5.2 Electrical capacitance

Figure 4.5 shows the plot of $(1/C(0) - 1/C(t))^2$ as a function of time, for water exposure at 100 °C and 100% relative humidity. Table 4.4 summarizes the results. The initial capacitance is 130 pF and the saturated capacitance is 158 pF. The thickness of the capacitor $h = 200$ nm $>> \sqrt{Dt}$ is assumed to be constant. $C(\infty)$ is obtained by saturating capacitors in the water bath for 23 hours at 100 °C. From the slope, the diffusion coefficient is measured to be 5.6×10^{-15}cm^2/sec. The diffusion coefficient matches with the value obtained by SIMS measurements within experimental error. The dielectric constant is calculated from the measured capacitance and capacitor dimensions. The reduced initial dielectric constant of 3.7 in table 4.4 is from error in top chromium electrode area during shadow mask sputtering. The concentration calibration factor K_ϵ that relates the dielectric constant to solubility is $K_\epsilon = 5 \times 10^{-21} \left(\text{molecules/cm}^3\right)^{-1}$.

4.5.3 Mechanical stress

Figure 4.6 shows the square of the change in average film stress, $(\sigma(t) - \sigma(0))^2$, as a function of time for a barrier held in a 100 °C boiling water bath. It follows a straight line, confirming that the diffusion coefficient is independent of H_2O concentration. The saturated stress is measured

Table 4.4: Electrical capacitance measurement at 100 °C and 100% relative humidity

Parameter	Value	Parameter	Value
$C(0)$	130 pF	ϵ_0	3.7
$C(\infty)$	158 pF	$\epsilon(x,\infty)$	4.5
Area	0.79×10^{-2} cm^2	K_ϵ	$5 \times 10^{-21} \left(\frac{\text{molecules}}{\text{cm}^3}\right)^{-1}$

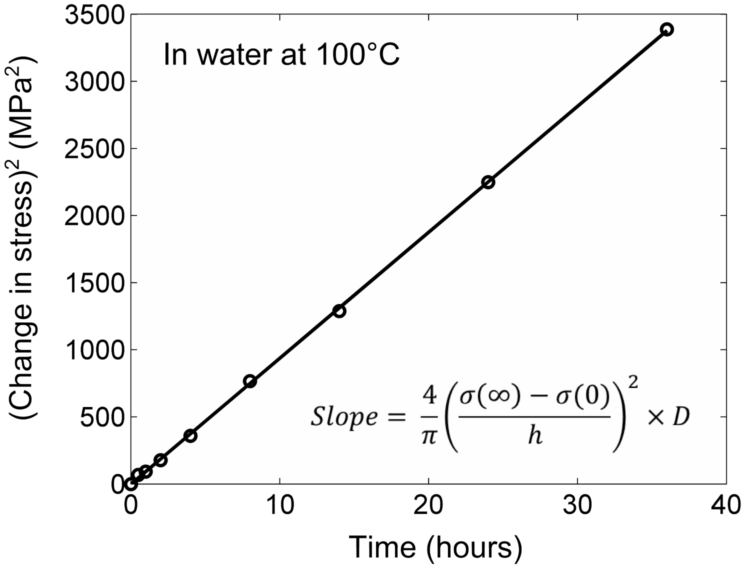

Figure 4.6: Square of the change in stress vs time in hours. The barrier layer was held in boiling water at 100 °C. The saturated stress was measured from water saturated 100 nm thick barrier. The saturated stress change is -325 MPa and hence diffusion coefficient is 4.4×10^{-15} cm^2/sec.

to be 325 MPa compressive on a 100 nm barrier saturated with water by holding it for 40 hours in boiling water. The diffusion coefficient is hence 4.4×10^{-15} cm^2/sec. This result matches well with the results obtained from SIMS analysis and capacitance measurements of 4.2×10^{-15} cm^2/sec and 5.6×10^{-15} cm^2/sec respectively. Calibrating the saturated stress against the dissolved water concentration obtained from SIMS, we get $K_\sigma = 2 \times 10^{-18}$ MPa/(molecules/cm^3).

4.5.4 Thermal activation energy

From the measurements of diffusion coefficient between temperatures 65 °C and 200 °C, we can evaluate its thermal activation energy using the mechanical stress measurement technique. Figure 4.7 is the plot of the diffusion coefficient of the barrier as a function of inverse temperature following

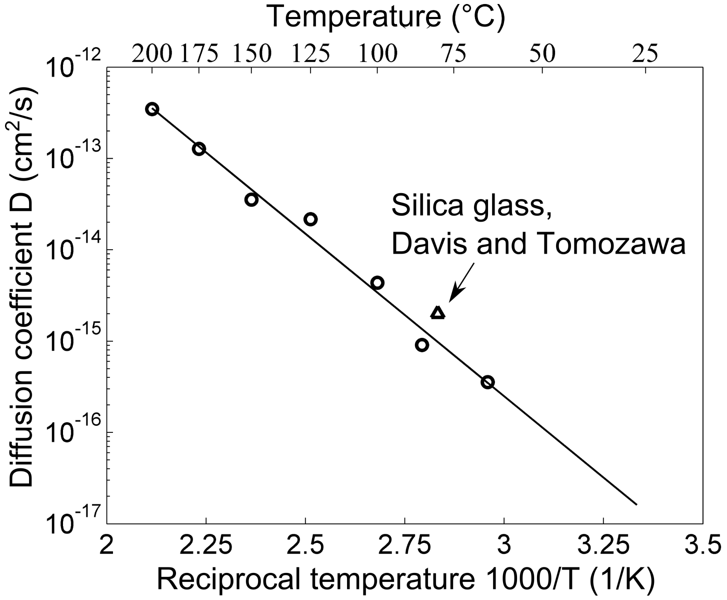

Figure 4.7: Arrhenius plot of the diffusion coefficient. The thermal activation energy determined from the slope is 0.71 eV. The triangle represents the data obtained by Davis and Tomozawa[61] for fused silica using, infrared absorption.

an Arrhenius distribution. The diffusion coefficient increases with temperature. The activation energy for the diffusion coefficient is measured to be 0.71 eV. The diffusion coefficient measured matches with the values measured in fused silica by Davis and Tomozawa by infrared absorption measurements[61] suggesting that the room temperature barrier layer performance is close to that of fused silica.

The saturated average stress, $\sigma(\infty)$, is measured at different temperatures. Using the calibration factor K_σ, $(\sigma(\infty) - \sigma(0))$ is converted to surface concentration n_0 or solubility S. Figure 4.8 gives the temperature dependence of solubility. The concentration is normalized to the water vapor pressure of 1 atmosphere. For temperatures above 100 °C,this pressure is established with 1 atmospheric pressure super heated steam. For temperatures below 100 °C the samples were held in a water bath. The solubilities S measured below 100 °C are divided by the saturated water vapor pressure at that temperature to obtain the solubility per atmosphere of water vapor pressure. Measurements below 100 °C, show that the saturated stress is proportional to the vapor pressure at a fixed temperature. Under the assumption that the saturated stress is proportional to the solubility with the same proportionality constant irrespective of the temperature, the solubility has

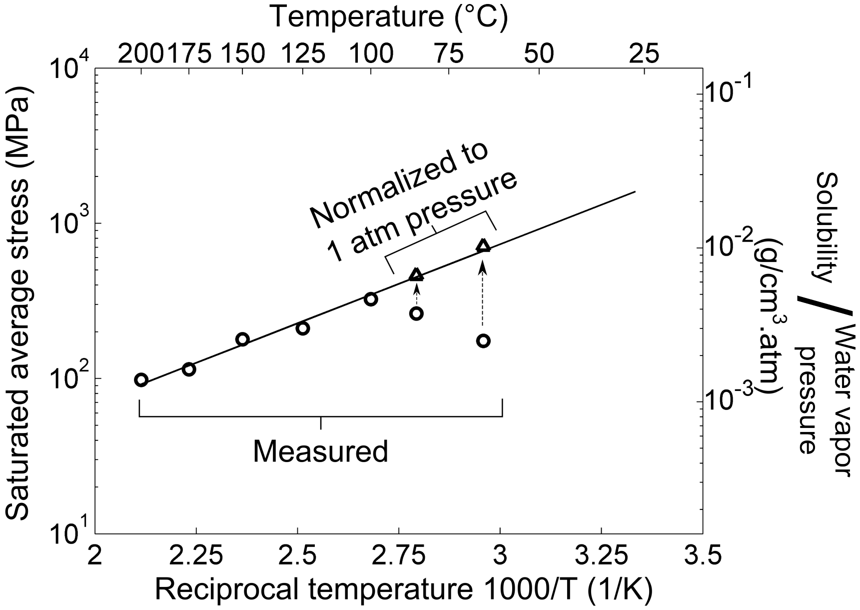

Figure 4.8: Arrhenius plot of saturated average stress and normalized solubility. The circles denote the saturated stress at 1 atmosphere water vapor pressure above 100 °C and at saturated vapor pressure below 100°. The triangles denote the saturated stress normalized to 1 atmosphere water vapor pressure. The line fit to the solubility of water has a thermal activation energy of -0.2 eV.

Table 4.5: Mechanical stress measurement at 100 °C and 100% relative humidity

Parameter	Value	Parameter	Value
$\sigma(0)$	-90 MPa	h	1500 nm
$\sigma(\infty)$	-415 MPa	E_D	0.71 eV
Substrate wafer	100 mm silicon $< 100 >$ orientation 525 µm thickness	E_{S_n}	-0.20 eV
K_σ	$2 \times 10^{-18}\ \frac{\text{MPa}}{\text{molecules/cm}^3}$		

an activation energy of -0.2 eV. For a given water vapor pressure, the solubility falls with rising temperature. Table 4.5 summarizes the parameters of all stress experiments.

4.6 Modeling the 1 monolayer permeation time

The permeation barrier is designed to protect the OLEDs for longer than 10 years under actual conditions of use. Such lifetimes are clearly too long for experimentation. The knowledge of the

Table 4.6: Barrier properties at different temperature and relative humidity (RH). WVTR, lag-time and 1 monolayer permeation time are calculated for a 3 μm thick barrier film.

	Diffusion Coefficient cm^2/s	Surface concentration mg/cm^3	WVTR $g/m^2/day$	Lag time	1 monolayer permeation time
Extreme operating condition:					
38 °C 90% RH	5.4×10^{-17}	0.97	1.5×10^{-7}	8.8 years	13.4 years
Accelerated test conditions:					
60 °C 90% RH	3.1×10^{-16}	3.6	3.2×10^{-6}	1.5 years	1.4 years
85 °C 85% RH	1.7×10^{-15}	3	1.3×10^{-5}	102 days	92 days

diffusion coefficient, its activation energy, the solubility and its activation energy gives us the power to extrapolate the barrier performance near room temperature. The properties of the barrier at a demanding operating condition and two accelerated test conditions are listed in table 4.6. For a 3 μm thick barrier, the steady state WVTR and lag-time are shown. The units for WVTR have been converted from molecules/cm^2/s to g/m^2/day.

Knowing the diffusion coefficients and solubility at a given temperature and relative humidity, the exact quantity of water diffusing into a barrier at any given time can be calculated using equation 4.4. The time, τ_{ML}, taken for 1 monolayer of water to permeate a 3 μm barrier at 100% relative humidity as a function of temperature is given by figure 4.9a. The acceleration factor from high temperature tests at 100% relative humidity to 38 °C 90% relative humidity is given in figure 4.9b. The acceleration factor is the ratio of time taken for 1 monolayer of water to permeate in high temperature test condition to the time at 38 °C 90% relative humidity.

The time taken for one monolayer of water to permeate through barriers of different thicknesses at the extreme operating condition of 38 °C 90% relative humidity is given in figure 4.10. The time taken does not go linearly with thickness as one might expect from equation 4.6 at first glance. This is because for the majority of time, the barrier is not in steady state condition, which takes the *lag-time* to reach it. The lag-time varies quadratically with the thickness as given by equation 4.7. As a result in our case, τ_{ML} varies with thickness with an empirically fitted exponent of 1.57

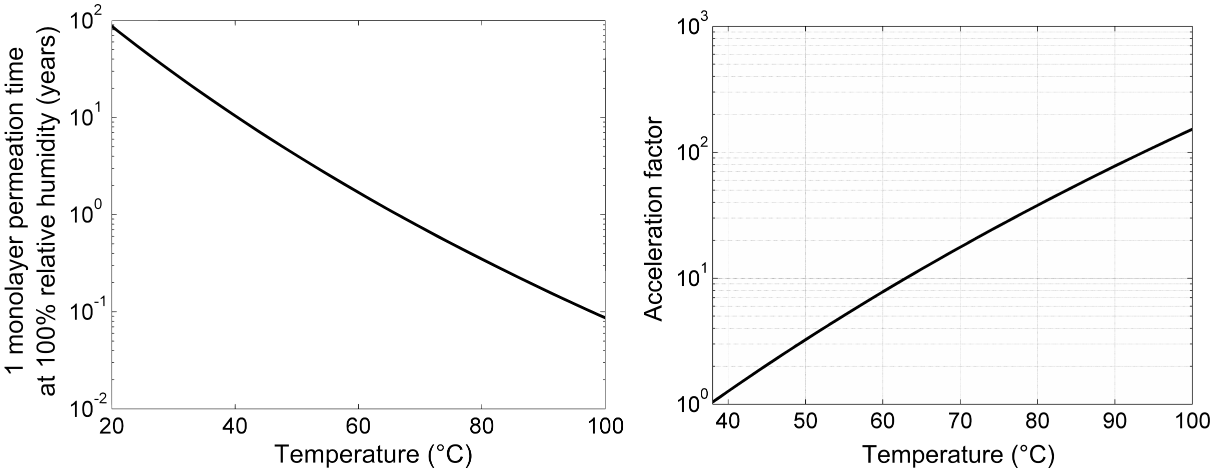

(a) Time taken for 1 monolayer of water to permeate a 3 μm barrier at different temperatures and 100% relative humidity.

(b) Acceleration factor for 1 monolayer of water permeation time from 38 °C 90% relative humidity to high temperature test conditions at 100% relative humidity for a 3 μm barrier.

Figure 4.9: 1-monolayer permeation time, τ_{ML}, and acceleration factor vs temperature.

.

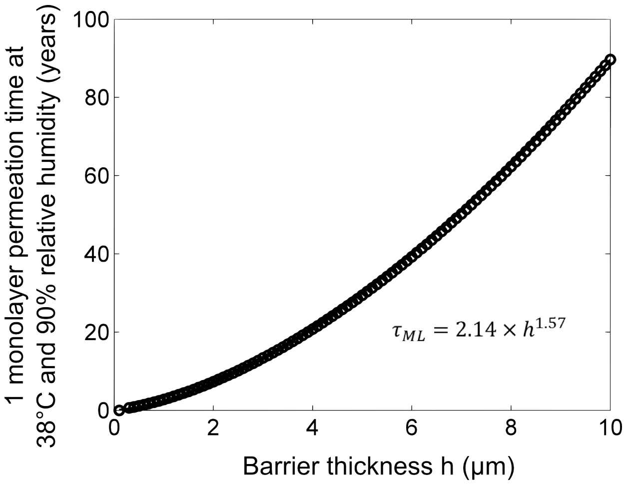

Figure 4.10: τ_{ML} dependence on the barrier film thickness. The lifetime scales exponentially with thickness with an exponent of 1.57.

for this barrier at 38 °C 90% relative humidity:

$$\tau_{ML} = 2.14 \times h^{1.57} \tag{4.23}$$

This example shows that the steady state water vapor transmission rate is a poor gauge for quantifying ultra-low barriers. Using τ_{ML} provides a more reliable gauge as it includes the effect of

Table 4.7: Calculated time taken for 1 monolayer to permeate through the hybrid barrier film for a range of film thicknesses.

Barrier thickness	Time τ_{ML} for permeation of 1 monolayer through a barrier film		
	T=85 °C, RH= 85%	T=30 °C, RH= 100%	T=25 °C, RH= 50%
100 nm	18 hours	160 days	1.6 years
200 nm	45 hours	346 days	4 years
500 nm	6 days	2.6 years	9 years
750 nm	11 days	4.3 years	13 years
1000 nm	17 days	6.1 years	19 years
1500 nm	31 days	11 years	30 years

lag time and WVTR. Once the diffusion coefficient and solubility for barrier materials at operating conditions are known a barrier that meets the required permeation target can be designed. Given a target of a maximum of 1 monolayer of water permeation over a 10 year device lifetime at 38 °C 90% relative humidity, a 3 µm thick barrier would have 1 monolayer permeation lifetime, τ_{ML}, of 13.4 years. Similarly other barrier materials can be characterized, and from the data new single layer or multilayer permeation barrier films can be designed to meet the desired target of water permeation. Table 4.7 shows the time taken for 1 monolayer to diffuse at 3 different conditions for different barrier thickness.

4.7 Conclusions

The permeation of water in a barrier can be characterized by monitoring the mechanical and electrical property changes induced by in-diffusion of water molecules. A SIMS measurement serves to calibrate the solubility of water in the barrier. The diffusion coefficient, diffusion thermal activation, solubility and solubility thermal activation is extracted from capacitance and film stress measurements. These parameters obtained under accelerated test conditions are used to predict the room temperature performance of the barrier. At 38 °C and 90% relative humidity a 3 µm thick barrier made of the hybrid material studied here, is predicted to have a 1 monolayer permeation lifetime, τ_{ML}, of 13 years. Similar measurements can be performed on other barrier materials to help design new single layer or multilayer permeation barrier films. In the following chapters, we improve the PECVD barrier further by deposition process tuning. Finally, we use the improved barrier material to create a multilayer barrier film for encapsulating bottom emitting OLEDs.

Chapter 5

Mechanism of water permeation

5.1 The mechanism of water diffusion in the barrier material

The hybrid barrier material has a chemical composition close to that of SiO_2 and, having been deposited from a glow discharge at nominal temperature is amorphous (refer appendix D). The plasma deposition process will introduce some hydrogen in the hybrid films and strained bonds. Because of the hybrid's similarity to fused quartz we surmise that water diffuses through the barrier by a mechanism that likely is similar to water diffusion in fused quartz. The diffusion of water in crystalline and fused quartz have been studied extensively. We adopt the analysis provided by Doremus[62] as it fits all of our results.

Experiments on the diffusion of H_2O into SiO_2 show that water enters by a diffusion-reaction mechanism. Two temperature regimes have been identified. At high temperatures, above 700 °C, the reaction of water with the Si-O-Si network *via*

$$\mathrm{Si{-}O{-}Si} + \mathrm{H_2O} \longrightarrow 2\,\mathrm{Si{-}O{-}H} \tag{5.1}$$

is fast. By enabling H_2O diffusion, the Si-O-H groups so formed dominate the rate of water diffusion. The network reacts with water first, thereby accelerating its diffusion. At low temperatures, the case we are studying, the fast process is diffusion of molecular H_2O, and local reaction with the Si-O-Si network follows. In other words, at low temperatures, the reaction is subsequent to diffusion.

The interaction of water with the hybrid at low temperatures can be treated as simple diffusion of H_2O molecules instead of reaction-diffusion.

In general, water enters the hybrid material by a diffusion-reaction mechanism in which five processes participate.

1. The surface concentration (activity) of water molecules $n(x = 0) = n_0$ equilibrates with the partial pressure (fugacity) of water p_{H_2O} in the surrounding atmosphere.
2. Water molecules diffuse into the solid from the surface.
3. The hydrogen (when soaked in H_2O) or deuterium (when soaked in D_2O) but not oxygen, of the diffusing water molecules exchanges with the hydrogen of the Si-O-H groups of the SiO_2: D_2O + Si-O-H $\longleftrightarrow$ HDO + Si-O-D.
4. The water molecules exchange oxygen in H_2O (or O^{18} in the case of H_2O^{18}) by insertion into the Si-O-Si bonds, which then re-connect: H-O^{18}-H + Si-O-Si $\longleftrightarrow$ H-O-H + Si-O^{18}-Si.
5. H_2O (or H_2O^{18}) molecules break Si-O-Si bonds permanently by insertion: H-O^{18}-H + Si-O-Si $\longrightarrow$ Si-O-H + Si-O^{18}-H.[1]

Our experiments show evidence for processes 1-4, with process 1 being immediate and processes 3 and 4 occurring in local equilibrium with the diffusing water molecules. Processes 1-4 alone will result in concentration independent diffusion mechanism. Process 4 is identified by tracking O^{18} isotopes. We shall also see that process 5 occurs only in a time scale so long that the process does not affect OLED protection.

5.2 Discussion of results

The hydrogen bonded in SiOH undergoes deuterium exchange with molecular H_2O or D_2O or DOH:

$$\mathrm{Si{-}O{-}H} + \mathrm{D_2O} \longleftrightarrow \mathrm{Si{-}O{-}D} + \mathrm{DOH}$$

$$\mathrm{Si{-}O{-}H} + \mathrm{DOH} \longleftrightarrow \mathrm{Si{-}O{-}D} + \mathrm{H_2O}$$

---

[1] process 5 is more likely to occur at strained Si-O-Si bonds.

This equilibration reaction is fast even at low temperatures and does not change the diffusion coefficient of DOH, H_2O and D_2O. The exchange results in generation of H_2O which diffuses out of the barrier from the top surface with the same diffusion coefficient as in-diffusing D_2O. The fall in concentration of hydrogen, and the complementary error function of hydrogen as a result of out-diffusion is observed in figure 4.3. The exchange process would suggest that at the surface where there is the source of D_2O, all the hydrogen should have been exchanged by deuterium. But instead, the surface concentration of hydrogen is 2.5×10^{20} atoms/cm^3. Some hydrogen atoms may be immobile and do not participate in the exchange reaction.

The same constant diffusion coefficient for both hydrogen and deuterium suggests that the water inside the barrier stays in the molecular form. This molecular water is subject to strong hydrogen bonding with the silicon dioxide network. The H during diffusion rapidly exchanges with SiOH or SiOD to establish local equilibrium. This complementary error function distribution suggests processes 1,2 and 3 operate as the water diffuses with a diffusion coefficient that is concentration independent. For this to be satisfied, the total number of SiOH+SiOD bonds should remain constant during the accelerated test. It is 6.5×10^{20} /cm^3. This result has been obtained earlier in fused silica and in quartz at low temperatures[55, 61].

The *erfc* concentration profiles suggest that molecular water does not break the Si-O-Si bridge and form two SiOH groups, as in equation 5.1 suggesting that process (5) does not operate. However, the exponential distribution of O^{18} in the H_2O^{18} soak tests (figure 4.4) suggests that O^{18} is incorporated into the SiO_2 network[62]. Since the *erfc* profile of the heavy water experiment rules out reaction diffusion (process 5), the oxygen 18 must be incorporated into the silicon dioxide network by a slow network exchange process (process 4), that leaves the network intact.

The carbon concentration measured in the film is 3×10^{20} atoms/cm^3 (table 4.2) and is constant as a function of depth. The value is less than the measured O^{18} concentration of 18×10^{20} atoms/cm^3. If O^{18} were to diffuse due to reaction with C to form CO_2, the O^{18} concentration must not increase more than twice the C concentration. The observation to the contrary along with the measured constant concentration profile of C suggests that the C atoms do not interact with the in-diffusing O^{18}.

The diffusion coefficient is independent of the thickness of the film and measurement technique. Both the capacitance measurement done on a 200 nm thick film and the stress measurement done on a 1 μm film, results in the same diffusion coefficient. The diffusion coefficient is also independent of the dissolved water concentration between temperatures 65 °C and 200 °C. The complementary error function, *erfc*, observed in SIMS, the quadratic change in inverse capacitance and the average stress over time imply no change in diffusion coefficient is independent of concentration. There is no evidence of reaction-diffusion mechanism.

In summary evidence points to processes (1-4) to happen and process (5) not to happen in our barrier films up to a temperature of 200 °C.

In the three groups of experiments, water would have to diffuse sideways from the edges of the sample over distances in the order of centimeters. This length is much larger than the top-down diffusion distance through the bulk of the barrier and reduces the likelihood of “sideways” interface diffusion affecting our results. The absence of deuterium at the bottom interface with the substrate in the SIMS experiments shown in figure 4.3 confirms the absence of interfacial diffusion.

Chapter 6

Particle encapsulation

Ideally a sub-micron thick hybrid layer will be enough to encapsulate a flat surface and prevent permeation. But in a real world device, the substrate accumulates particles. These particles can affect the profile of the deposited film such that the film becomes permeable. The reason is explained below.

Consider a particle sitting on the substrate during the barrier deposition step. When the substrate surface faces the plasma, a particle lying on the substrate creates two kinds of surfaces:

1. Exposed surfaces - surfaces directly in contact with the plasma.
2. Unexposed surfaces - surfaces not directly in contact with the plasma.

The region below the particles is an unexposed surface. It shadows the plasma partially or completely. The plasma deposition process can be directional. In this respect PECVD is closer to physical vapor deposition (PVD) in vacuum than to chemical vapor deposition (CVD) at some elevated pressure. In CVD, growth can be made uniform over all surfaces. In plasma deposition, the layer may deposit primarily on the exposed surfaces that face the plasma.

One might argue that the precursor molecules HMDSO and oxygen reach all surfaces evenly, and hence layer growth should be uniform and CVD-like growth. But in a PECVD process, the precursor molecules do not directly contribute towards growth. Rather the reactive radicals generated in the plasma contribute to the deposition (chapter 3). The plasma exists between the powered electrode and the grounded gas ring. The reactive species that originate in the plasma travel directionally away from this plasma region. They have long mean free paths, which makes their trajectories directional. This results in growth only on the exposed faces which see the plasma and results in a profile that may resemble that obtained in a PVD like process.

This anisotropy in growth over a particle becomes critical for its encapsulation. Let us assume the case of a particle in the shape of a sphere with a diameter of 5 µm, sitting on an OLED substrate. In PVD, the substrate region below the particle is shadowed during the deposition by the particle. Partial film deposition happens in this shadow region. To encapsulate the particle, the entire particle has to be buried under the film. To bury the 5 µm size particle, a PVD film must be grown to a thickness of at least 2.5 µm. At 2.5 µm the film that is deposited on the exposed substrate come in contact with the equator of the sphere-particle. To first order this means that we need a film at least half as thick as the spherical particle to close a break in the layer caused by the shadow of the particle. It is easy to understand that making a reliable seal will require a layer that is thicker than half the diameter of the spherical particle.

6.1 Deposition on standard test particles

To understand how a particle is encapsulated by the hybrid barrier layer, to identify the layer thickness required, and to establish a reliable model for the encapsulation process, we perform deposition on standard test particles with well-defined geometries. Layers are grown on substrate surfaces with these standard particles. Growth conditions are varied, and cross sections of substrate/particle/layer are examined with a scanning electron microscope. Particular attention is paid to layer continuity over the particles. Two test "particle" structures are used in understanding the film growth over a particle:

1. Microfabricated T-shaped ridges.
2. Dispersed glass fibers.

A third type of particle, glass bead spheres with 5 µm diameter is used for a separate study in chapter 8.

6.1.1 T-Shaped ridges

The first standard "particles" are T-shaped ridges micro-machined on a silicon wafer substrate. Similar T-shaped structures have been fabricated, to model depositions from Low Pressure CVD, Plasma Enhanced CVD and Sputter deposition[63, 64]. Silicon is chosen as the substrate for two reasons. 1. Microfabrication on silicon is straightforward in Princeton University's nano / microfabrication facility to obtain reproducible, uniform structures. 2. Silicon gives a good cleaving plane and that enables sharp cross-sections for viewing in the SEM. Figure 6.1 is a schematic rendering of the T-shaped ridges fabricated on the silicon substrate. The character of artificial particles comes out best in a cross section like that of the inset. The three regions in the cross section are 1. Hat, 2. Stalk and 3. Substrate. We will use these terms in the discussion of hybrid layer growth below.

Fabrication of T-Shaped ridges

We start with a 4-inch diameter silicon wafer that is covered with 1.0 µm silicon dioxide made by wet oxidation and 500 nm of polysilicon on top. The top polysilicon is patterned by photolithography and is etched in a Samco 800 Reactive Ion Etcher. A Bosch process is used to obtain steep side walls. The etched pattern is aligned in such a way that, once the wafers are fabricated, it can be diced into many identical substrate samples. After etching the polysilicon hats, the photoresist is stripped and the wafer is dipped into 1:10 buffered oxide etch for 30 minutes to etch the silicon dioxide. The polysilicon hats act as the mask for this step. The buffered oxide etch etches the silicon dioxide isotropically, which results in a deep undercut. The etching is stopped such that the remaining silicon dioxide forms the stalk of the T. Now we perform an RCA clean[1] and grow 65 nm of "dry" oxide. The dry oxide makes the substrate, stalk and hat surfaces close to that of silica glass. The wafer is diced into many pieces with a dicing saw. Each piece is used as a substrate for a separate experiment.

Figure 6.2 is a SEM cross section that shows the right half of a T structure. The silicon substrate, the silicon dioxide stalk and the polysilicon hat are identified. The polysilicon hat is bent due to the built-in stress of the polysilicon layer.

---

[1] RCA clean: 1. Acetone clean; 2. Organic removal: 15' in 1:5 NH_4OH:H_2O at 70 °C; 3. Oxide clean: 3' in 1:100 HF; 4. Metal clean: 15' in 1:1:5 H_2O_2:HCl:H_2O at 70 °C; 5. Oxide clean: 3' in 1:100 HF.

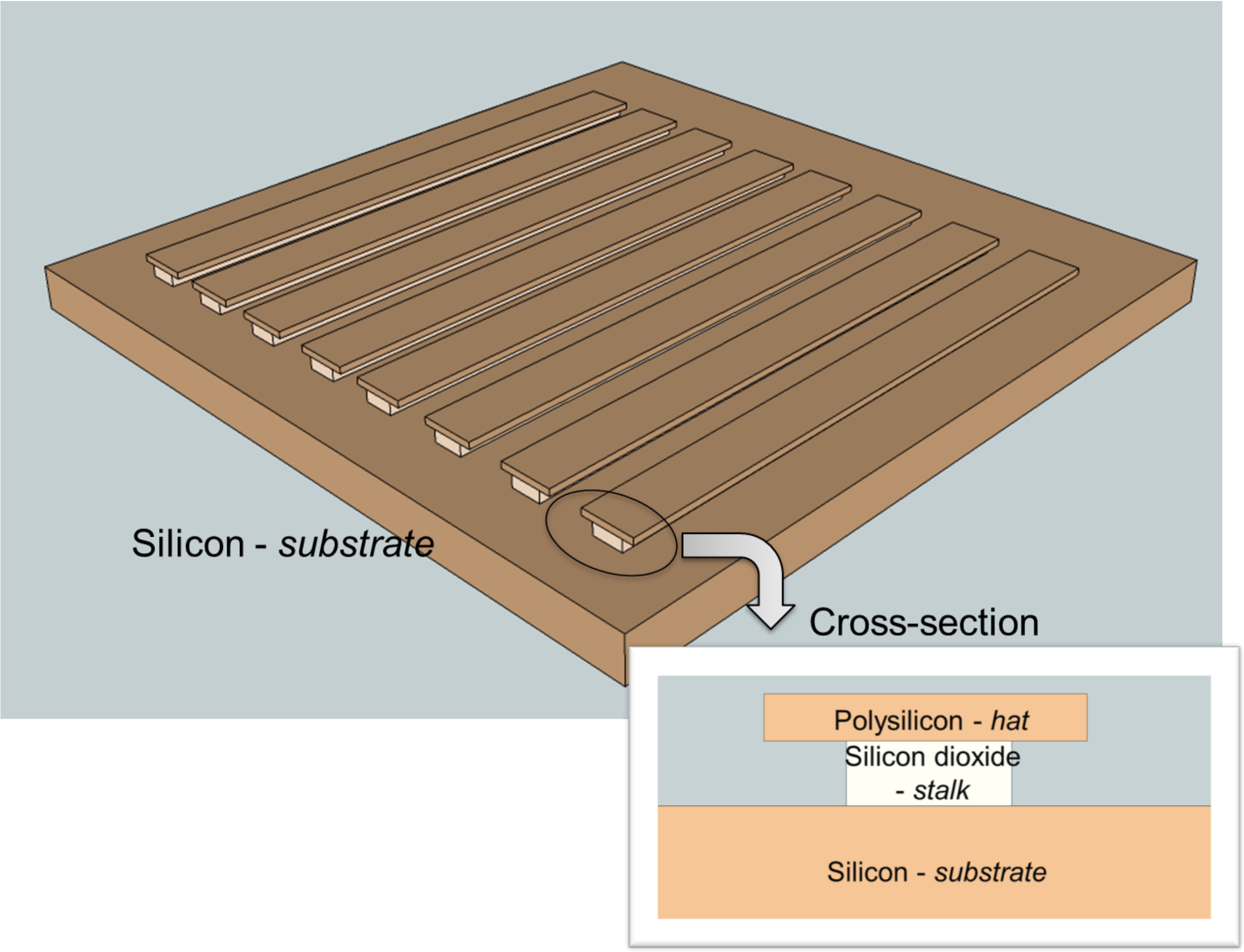

Figure 6.1: Schematic of the silicon substrate containing fabricated artificial T-shaped particle - not drawn to scale.

Depositions on T-shaped ridges

Depositions are performed on this T-shaped artificial particle. The standard film is deposited at the following conditions: gas flow rates HMDSO 1.1 sccm, oxygen 33 sccm, gas pressure 110 mTorr, plasma power 70 W, substrate at room temperature (table 3.2). Figure 6.3 shows the cross section taken in a SEM after deposition.

The cross section of figure 6.3 shows two distinct features: 1) The deposition is a PVD like. There is growth on top of the hat and minimal growth on the underside of the hat. Also, there is minimal deposition on the substrate region that is shadowed by the hat. 2) Near the edge of the hat, there are two growth fronts; one grows on top of the hat, and two, from the exposed part of

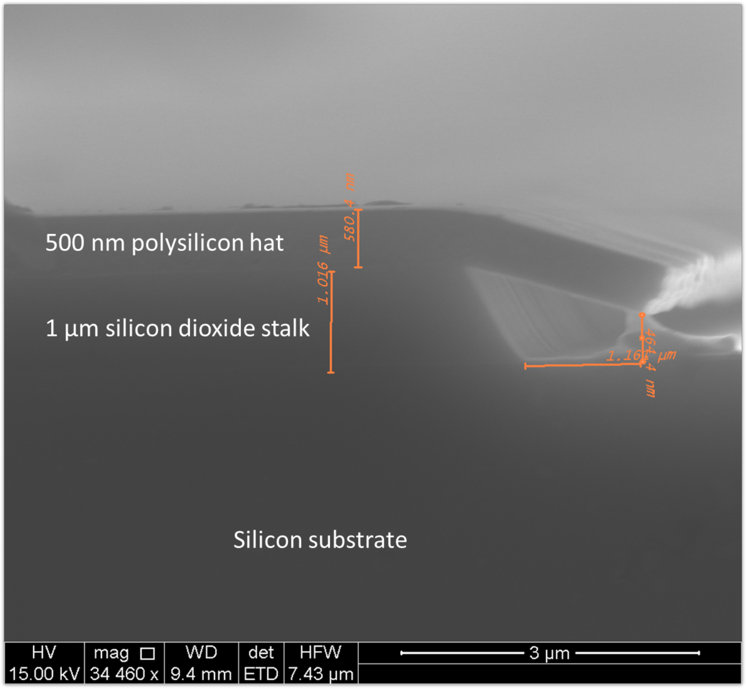

Figure 6.2: Scanning Electron Microscope (SEM) image showing the right half of the artificial "particle" on silicon substrate. The particle has a 1 µm silicon dioxide stalk and a 500 nm polysilicon hat. The polysilicon hat and the silicon substrate are coated with a dry silicon dioxide of thickness 60 nm.

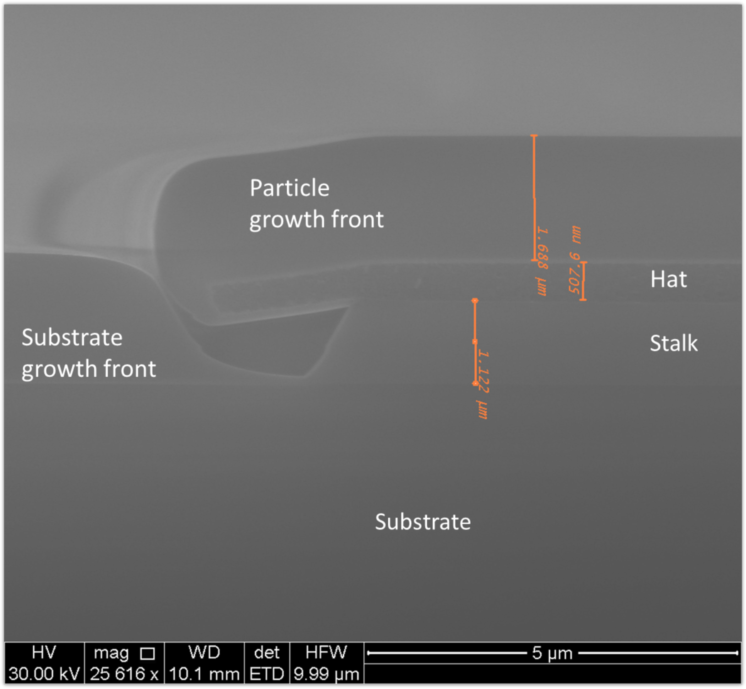

Figure 6.3: Cross section SEM image of the artificial T shape particle after the growth of a standard film (HMDSO 1.1 sccm, oxygen 33 sccm, 110 mT, 70 W). The image shows the growth on the particle and the growth on the substrate do not touch after a deposition of 1.6 µm of hybrid layer.

the silicon substrate. The growth fronts do not touch each other. They stay separate and the gap is termed the *chimney*.

The unexpected feature in figure 6.3, *the substrate and particle growth fronts not meeting*, has profound impacts on encapsulation. Let us consider a situation where the substrate is an OLED instead of silicon, and the T shape is an unwanted dust particle sitting on top of the OLED. Now if this OLED were to operate in the real world, air and moisture would pass through the gap between the particle growth front and the substrate growth front and would reach the OLED at the base of the particle. This OLED would develop a black spot at the location of the particle.

The hat is bent by built-in stress in the polysilicon layer. Therefore the edge of the hat near the edge lies lower than the hat's surface directly above the stalk. The lower edge of the T lies 700 nm above the substrate. Intuitively, one would expect the hybrid layer that grows on the substrate to touch the edge of the hat once the hybrid layer has reached a thickness of 700 nm. And when it has reached a thickness of 1.2 μm it should encapsulate the entire T, because 1.2 μm is the height from the substrate to the top of the hat at its edge. But in figure 6.3 even after a film growth of 1.6 μm, the film has not yet encapsulated the particle. In fact, the layer that grows on the substrate is receding away from the T. A much thicker film appears to be necessary for encapsulating the T (and hence protect an OLED).

What happens when a thicker hybrid layer is grown? Figure 6.4 shows the deposition profile after a long deposition. The growth fronts on the substrate and on the T merge at a thickness of 2.3 μm to form a continuous layer.

While most of the species that contribute to film growth arrive perpendicularly to the substrate, they have a *distribution in angle.* After they have attached themselves to the surface they may undergo *surface diffusion.* Due to this directional distribution incoming species and surface diffusion, as the growth proceeds, the layer deposited on the top of the particle becomes wider than the particle itself and casts an increasingly bigger shadow. Monte-Carlo simulations showing these phenomena are discussed in the last part of this chapter.At the start of the deposition the shadow cast on the substrate has the same size as the polysilicon hat. This means that the surface area that is not directly exposed to the plasma increases during the deposition. This increase in the size of the shadow results in a *chimney* that travels up and away from the particle edge before it is sealed.

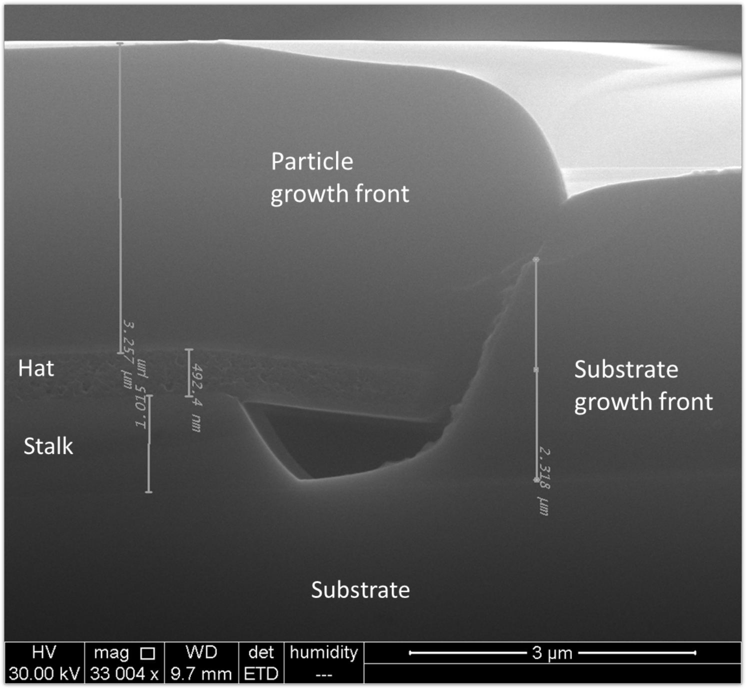

Figure 6.4: Cross section SEM image of the T shape artificial particle with a standard barrier film (HMDSO 1.1 sccm, oxygen 33 sccm, 110 mT, 70 W). The particle growth front and substrate growth front join at a height of 2.3 µm to form a conformal layer. The total deposited film thickness is 3.2 µm.

The chimney is visible in figure 6.4 and a pronounced case in which the growth fronts on the substrate and on the T stay apart because of shadowing is shown in figure 6.5. This particular 2 µm hybrid film is grown at a very high deposition rate in a diode configured PECVD. The two growth fronts are separated by a wider chimney.

The chimney must be sealed with the shortest growth procedure possible. To identify the recipe for hybrid growth that encapsulates the T in the shortest time, and smallest thickness, the growth parameters: HMDSO flow rate, oxygen dilution, power, and pressure are varied to identify changes in the growth profile. We carried out many experiments to identify the optimal conditions. For clarity only the recipe modifications that closed the chimney faster than the growth of the standard hybrid layer are described. We found that the plasma power and deposition gas pressure affect the rate of chimney closing.

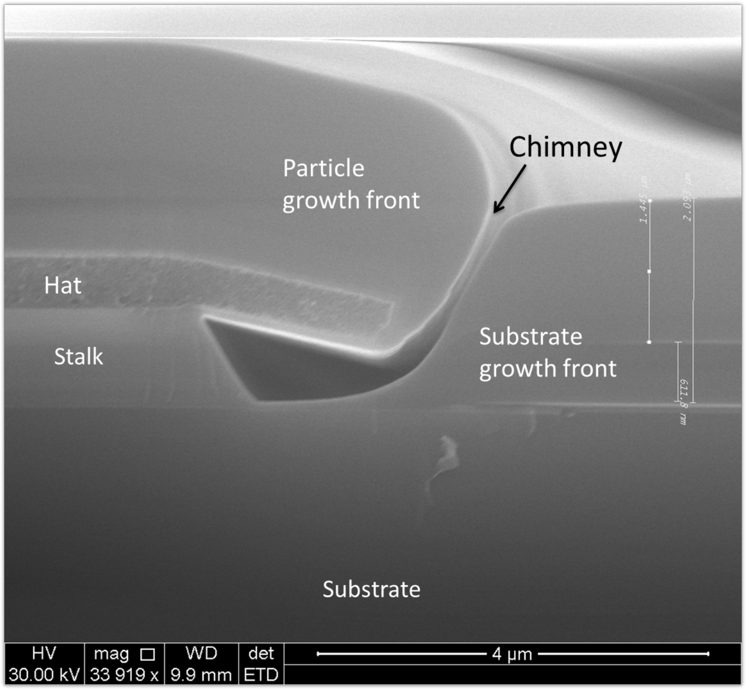

Figure 6.5: SEM cross section of a high rate deposition layer showing a wider chimney.

Deposition pressure and power

Increasing the pressure and reducing the power greatly changes the growth profile. Figure 6.6 shows a film that is grown at conditions: HMDSO 1.1 sccm, oxygen 33 sccm, 500 mT, 30 W (standard hybrid: HMDSO 1.1 sccm, oxygen 33 sccm, 110 mT, 70 W). The layer deposited at this condition from here on is referred to as the *high pressure layer*. Increasing the pressure reduces the mean free path of the active species in the plasma region. If the path becomes too small particles will form in the gas phase. Reducing the power compensates this effect to some extent. A 1.7 µm layer is grown in 1 hour. The deposited layer has high tensile stress, which causes the layer to delaminate. The high pressure growth conditions cause a significant amount of undergrowth of 187 nm thickness in the unexposed region. In the standard layer the undergrowth is 80 nm thick, which suggests that increasing the pressure makes the layer more uniform between the exposed and unexposed regions. The two growth fronts have merged to form a continuous layer at a height of 1.2 µm from the substrate surface. Overall these observations suggest that the layer grown at high pressure can seal the chimney. But it is highly strained and adheres poorly to the substrate (which is coated with thermally grown SiO_2).

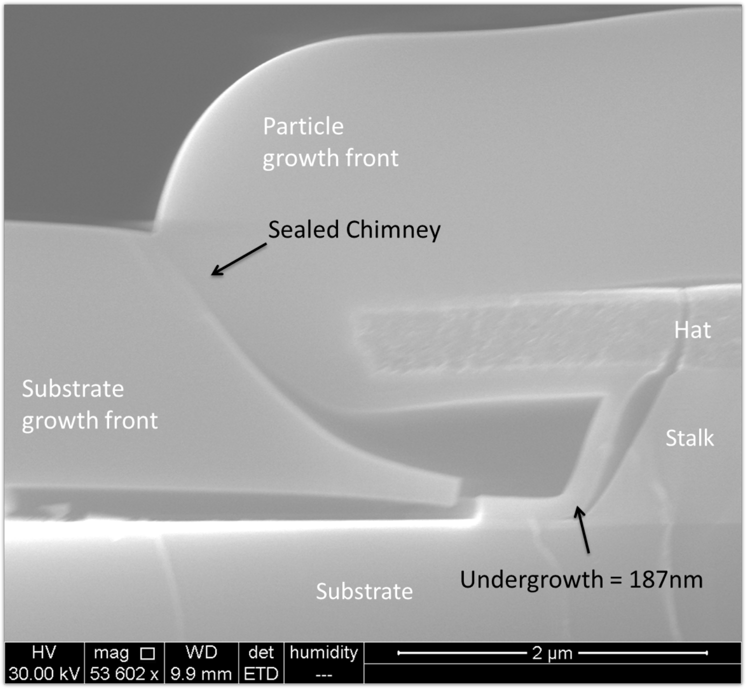

Figure 6.6: *High pressure* deposition (HMDSO 1.1 sccm, oxygen 33 sccm, 30 W, 500 mT). The layer thickness is 1.7 μm. The undergrowth is 187 nm.

Multilayer deposition

We created multilayer films to prevent delamination in the high pressure layer. Two different kinds of film are grown.

First a bilayer film is fabricated. The bilayer has 1.2 μm *standard layer* followed by a 1.3 μm *high pressure layer*. SEM cross sections are shown in figure 6.7a. Figure 6.7b suggests that the chimney begins to close right at the start of high pressure growth, which again suggests that growth at high pressure is a good technique for sealing a chimney. But the high pressure layer again peels off, this time off the standard film as seen in figure 6.7a. The stress also cracks the high pressure film, see the top of the T figure 6.8.

Comparing figure 6.8 with figure 6.6 we find that the adhesion of the high pressure layer to the standard layer is not any better than its adhesion to the thermal-SiO_2 coated substrate itself. The cracks occurred after the substrate was removed from the plasma deposition chamber. At the end of a deposition, the sample is allowed to cool. Then it is taken out of the chamber. While coming out of the chamber its surface is smooth and free of cracks. But then the encapsulation layer starts to crack, and within minutes cracks appear over the entire layer. Figure 6.8 shows the SEM top view of the T structure with many cracks. Small temperature swings that happen while venting the chamber raise the film stress resulting in the development of cracks.

To confirm that the high pressure layer is stressed and cracks on exposure to air, the layer growth conditions were modulated to form a three layer film:

1. A bottom 930 nm standard layer: 110 mTorr, 70 W.
2. A middle 1.2 μm high pressure layer: 500 mTorr, 30 W.
3. A top 450 nm standard layer: 110 mTorr, 70 W.

The cross section of the layer is shown in figure 6.9a. The top, 450 nm standard layer prevents the cracking of the middle layer due to tensile stress. As in figure 6.9a the chimney closes as the conditions are changed from standard to high pressure film at a height of 930 nm. The third top layer, grown again under standard conditions, holds the middle portion in place without cracking as seen in figure 6.9b. The top layer stays conformal like the middle layer The standard layer of 6.4 had to be made 2.3 μm thick to seal off the chimney. In the case of the sample of 6.9b, at 930 nm height the chimney is sealed to give a conformal surface.

These results point to a technique for particle encapsulation in which the pressure is increased and the power is reduced for part of the deposition. The constraint is that the portion of the barrier layer grown at high pressure must be thin. Samples like the one in figure 6.5, where the chimney is wide, require a thick high pressure portion to plug the chimney. But samples with a narrow chimney as in figure 6.3 require only a thin high pressure portion to plug the chimney, after which we can resume growth under standard conditions. To make the technique more generally applicable, we evaluate barrier coatings deposited on a different type of particle, pieces of glass microfibers.

6.1.2 Encapsulating glass micro-fibers

T shaped structures are highly useful for quickly exploring different deposition recipes and for identifying the right conditions for particle encapsulation. Because of its overhang, the T shaped structure is very challenging to encapsulate. A typical dust particle is more spherical than a T; it is not as unfavorable to encapsulate as a T shaped structure is. Therefore we tested the multilayer

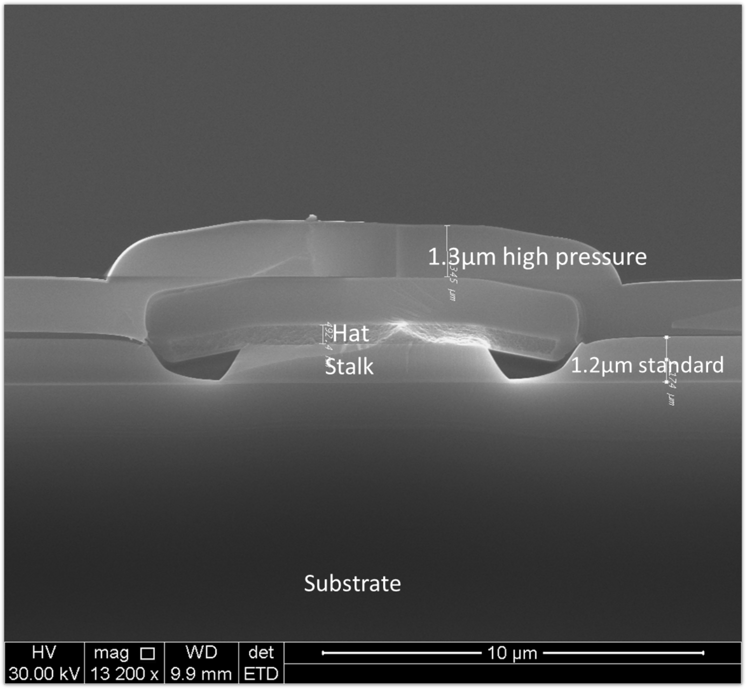

(a) 1.2 µm standard layer followed by a 1.3 µm high pressure layer.

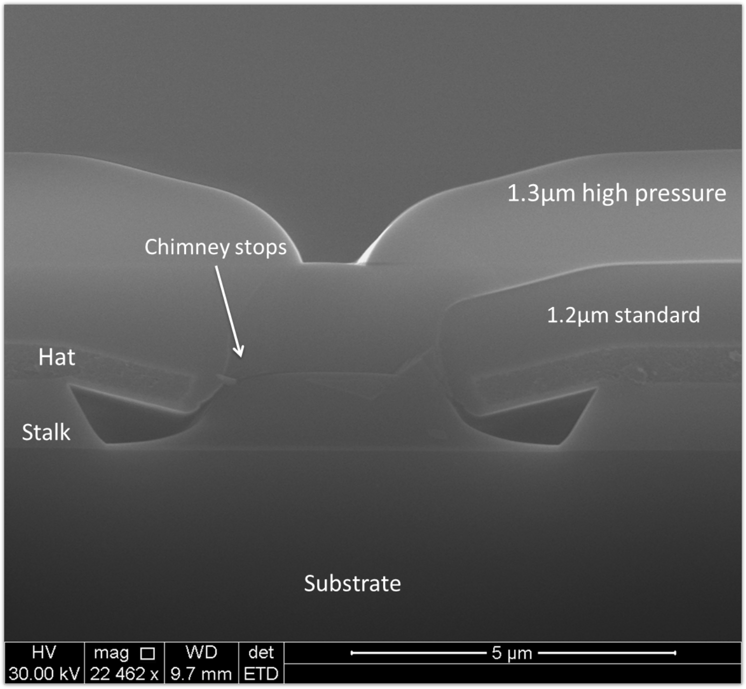

(b) The chimney closes as soon as the high pressure layer growth starts.

Figure 6.7

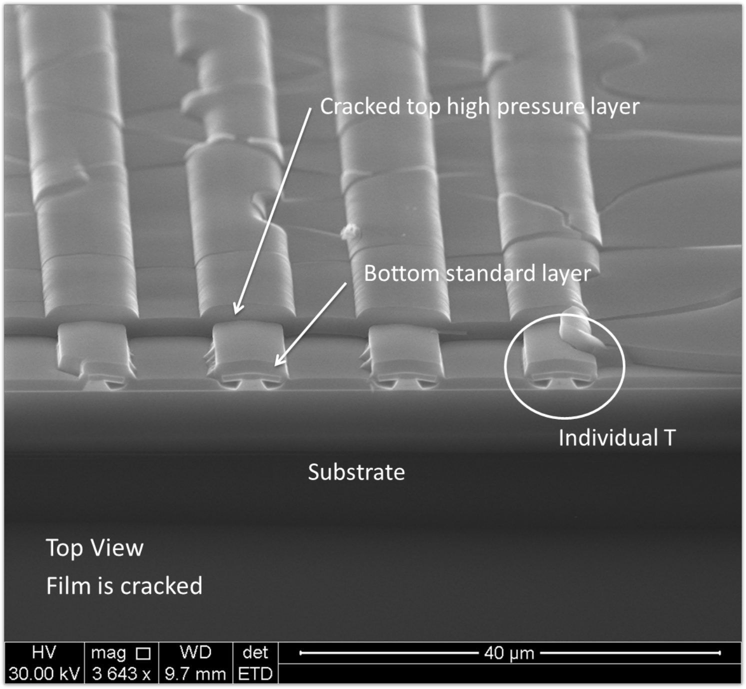

Figure 6.8: SEM top view showing cracks in the high pressure layer.

structure on glass microfibers, which is a step closer to a typical particle that one might find on an OLED display.

Glass microfibers are known in the electronics industry for their application as LCD spacers. Meshes made out of microfibers are used for manufacturing of chemically inert filters in large quantities. Very large quantities of fiber are used for thermal insulation products. A batch of fibers from the Johns Manville Corp. was obtained (product number 212x). The glass fibers have diameters that range from 3 μm to 7 μm.

Preparation of substrates with glass micro-fibers

A silicon wafer is diced into 1.5 cm× 1.5 cm square pieces. Each square piece acts as a separate substrate. A tweezer full of the glass fibers is taken and is tapped on top of the silicon substrate, to sparsely cover with fibers. The fibers are pressed against the silicon substrate with a glass slide. This is done to conformally spread the fibers. Now we perform the required depositions and then the silicon is cleaved into two pieces that are analyzed in the SEM. Cleaving the silicon wafer breaks some of the glass fibers across the cleaving edge, along with the encapsulation layer. In the SEM we search for such split fibers and encapsulant and capture their cross section.

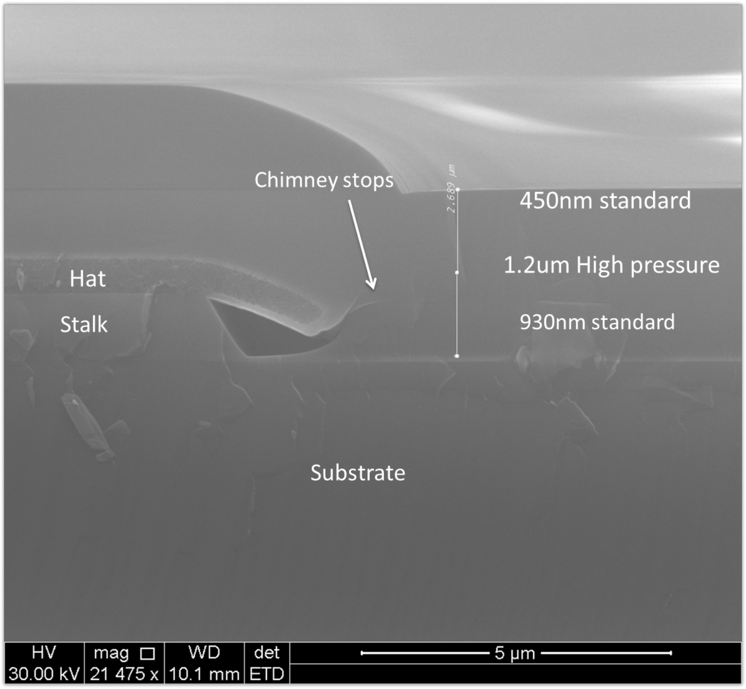

(a) Three layer film: 1. 930 nm standard, 2. 1.2 µm high pressure, and 3. 450 nm standard. The chimney closes at the start of high pressure layer.

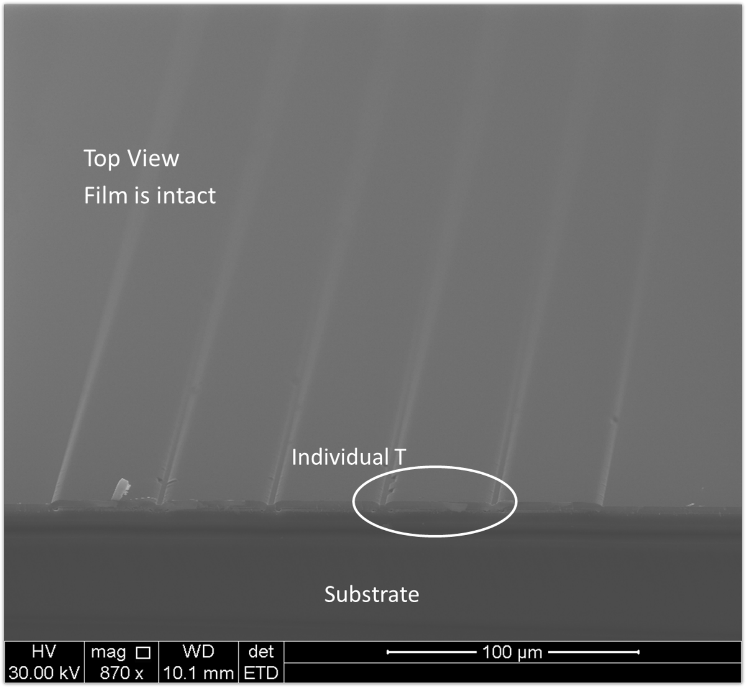

(b) Top view showing an intact, crack-free layer encapsulating a series of T structures.

Figure 6.9

The tapping distributes the glass fibers randomly on the surface of silicon. There are thousands of these fibers in a single 1.5 cm× 1.5 cm silicon sample. Electrostatic attraction keeps the smaller fibers attached to the substrate throughout the deposition. To improve the adhesion of thick fibers, which sometimes break off during the cleaving for SEM inspection, a thin photoresist layer is spun on the silicon substrate before the fibers are distributed. The photoresist is then allowed to outgas on a hot plate before starting the deposition. The photoresist makes the fibers adhere sufficiently well during cleaving.

Depositions on glass micro-fibers

Figure 6.10a shows such a cross section obtained by cleaving. In this experiment, a 5 μm standard layer (HMDSO 1.1 sccm, oxygen 33 sccm, 110 mT and 70 W) is deposited. The figure shows a 3 μm diameter glass fiber plus the 5 μm thick encapsulation layer grown on top of the fiber.

Pressing the glass fibers against the substrate is important. The glass fibers are not straight and are not rigid. They have a structure resembling that of a flexible thread. As a result glass fibers just sprayed on top of the substrate curve up from the surface forming random shapes. Because of these squiggles, each of the glass fibers makes contact with the substrate only at a few points. So when we take a cross section, if we happen to cleave at the right point (which is very rare), we have a small chance to get a SEM of the glass fibers touching the substrate. Otherwise we obtain a glass fiber which is lifted off the surface like the one in figure 6.10b. In the figure, right at the cleavage plane, the 2.7 μm diameter glass fiber can be seen lifted from the substrate. The cylindrical portion of the fiber behind the cleavage plane shows the fiber being lifted further off the substrate. To avoid this problem, a glass slide was placed on top the substrate with fibers and pressed with a uniform force to flatten them before deposition. Pressing the glass fibers against the substrate increases the number of contact points, stretches the length over which the fiber makes contact with surface, and improves the chances of getting a useful SEM cross-section.

Modulation of Pressure and Power

Figures 6.10a and 6.10b show standard layers deposited on glass fiber containing silicon substrates. Figures 6.11 and 6.13 show a 5.6 μm thick film encapsulating a 3.5 μm glass fiber. Figure 6.12 is

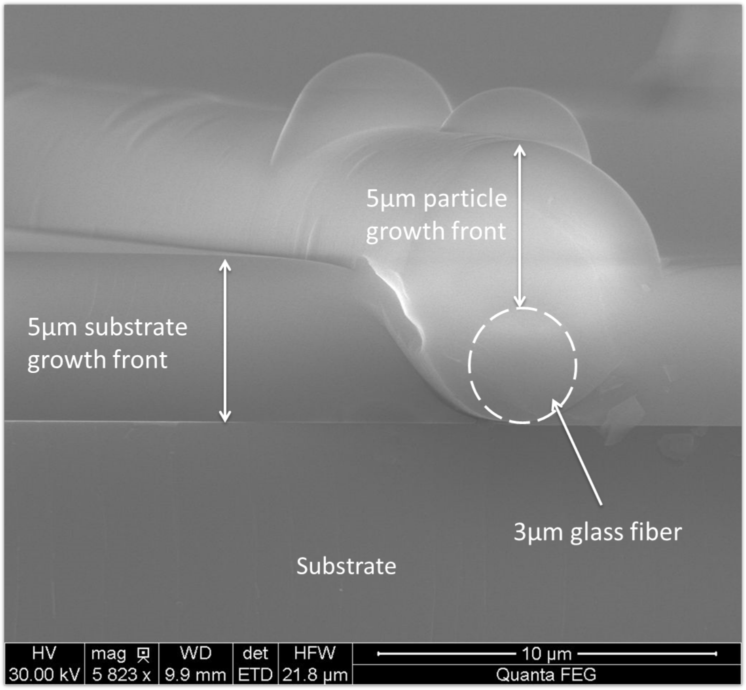

(a) 3 µm cylindrical glass fiber encapsulated by a 5 µm barrier layer. The glass fiber runs into the plane of the paper.

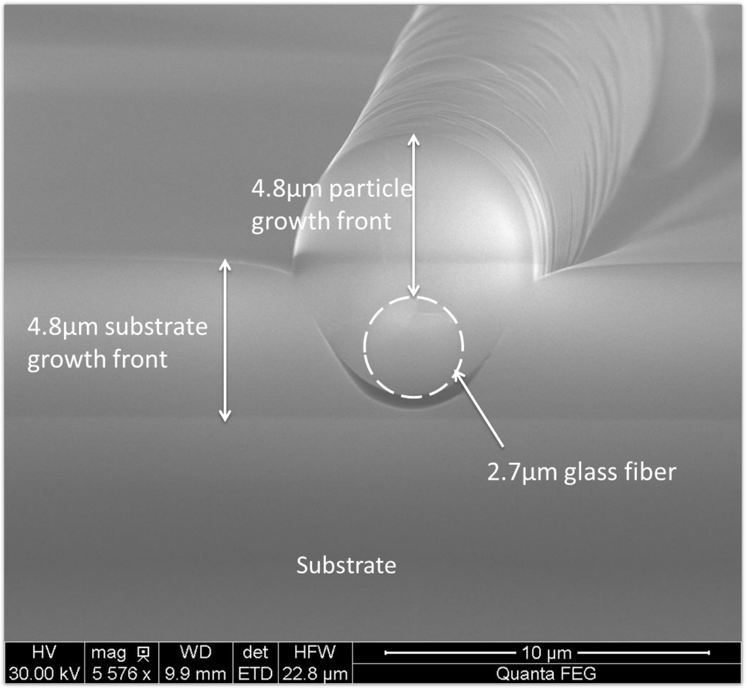

(b) 2.7 µm glass fiber with a 4.8 µm barrier on top. At the cleave the cylindrical rod is lifted off the substrate. Further back (into the plane of the paper) the cylinder is seen to lift off the surface even more.

Figure 6.10: Barrier film deposition on glass fibers.

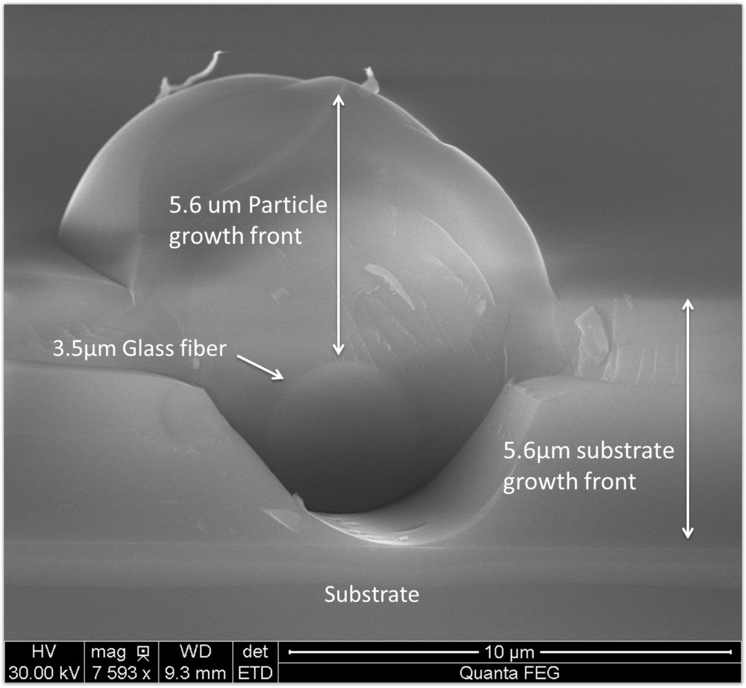

Figure 6.11: Three layer film deposition on a glass fiber: 3.7 μm standard deposition followed by 700 nm high pressure deposition and then 1.2 μm standard deposition, encapsulating a 3.5 μm glass fiber.

an illustration of the 3.5 μm glass fiber having been encapsulated. The film has three layers and the growth sequence from bottom to top is as follows:

1. 3.7 μm standard deposition: HMDSO 1.16 sccm, oxygen 33 sccm, 110 mT, 70 W, 2.5 hours.
2. Cool for 30 minutes in atmosphere after venting the chamber.
3. 700 nm high pressure deposition: HMDSO 1.16 sccm, oxygen 33 sccm, 300 mT, 30 W, 1 hour.
4. 1.2 μm standard film: HMDSO 1.16 sccm, oxygen 33 sccm, 110 mT, 70 W, 1 hour.

The first deposition under standard conditions takes 2.5 hours to produce 3.7 μm. To prevent overheating of the sample by the plasma, it is allowed to cool down in atmosphere for 30 minutes before continuing growth. The second deposition under high pressure layer that plugs the chimney and the third deposition standard layer are deposited in succession. In figure 6.11 only two portions are distinguishable. The bottom portion corresponds to the first growth. The top portion corresponds to the second high pressure and the third standard portions fused together.

In this structure, unlike the T shaped structure, the chimney is very thin to begin with and appears to exist during standard deposition conditions. In the second, high pressure, conditions

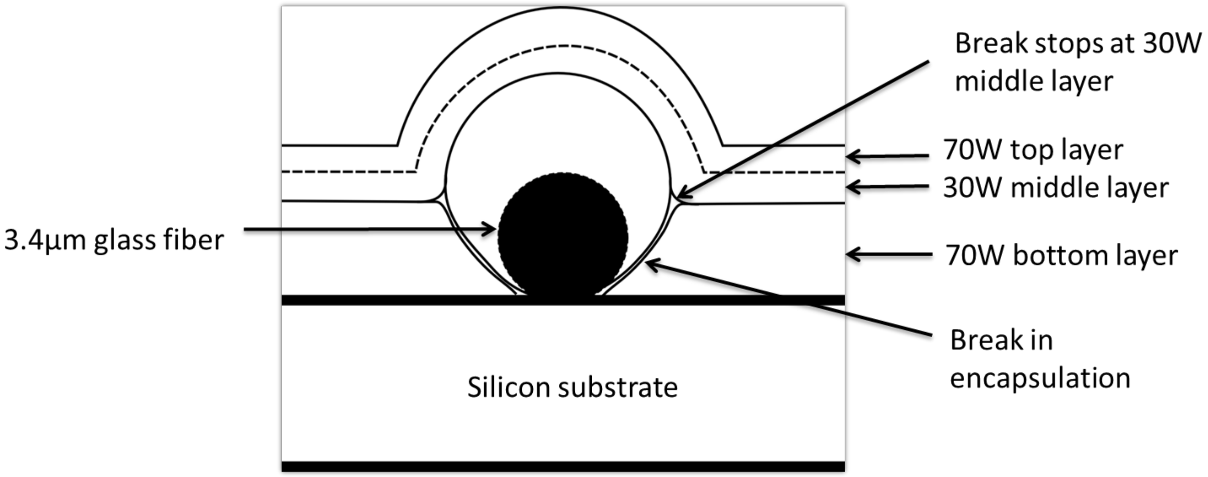

Figure 6.12: Schematic of the three layer film on a glass fiber: 3.7 μm standard deposition followed by 700 nm high pressure deposition and then 1.2 μm standard deposition, encapsulating a 3.5 μm glass fiber.

the chimney is sealed and the entire film becomes completely uniform. The way in which the encapsulating barrier layer grows along the circumference of the glass fibers provides information on the strength of the layer under modulated growth conditions.

Careful inspection of figure 6.13 shows the end of the glass fiber, which has broken not right at the cleavage plane of the silicon but slightly behind it (i.e., into the plane of paper). The complementary piece of the fiber took along with it the barrier layer that grew on the fiber, plus parts of the second and third portions of the barrier layer that grew on the substrate. This observation allows establishing the relative strengths of the interfaces:

1. The standard barrier layer adheres strongly to the glass fiber and to the substrate.
2. The first (standard) portions of the barrier layers on the fiber and on the substrate form the chimney. The chimney is a weak interface.
3. The barrier layer has a weak plane between the first and the second layers from the bottom.
4. The second and third layers from the bottom are continuous over the fiber and the substrate; no weakness can be seen between these layers on fiber and substrate.

Figure 6.14 shows a 6.5 μm glass fiber encapsulated with an 8 μm layer. The growth sequence from bottom to top is as follows:

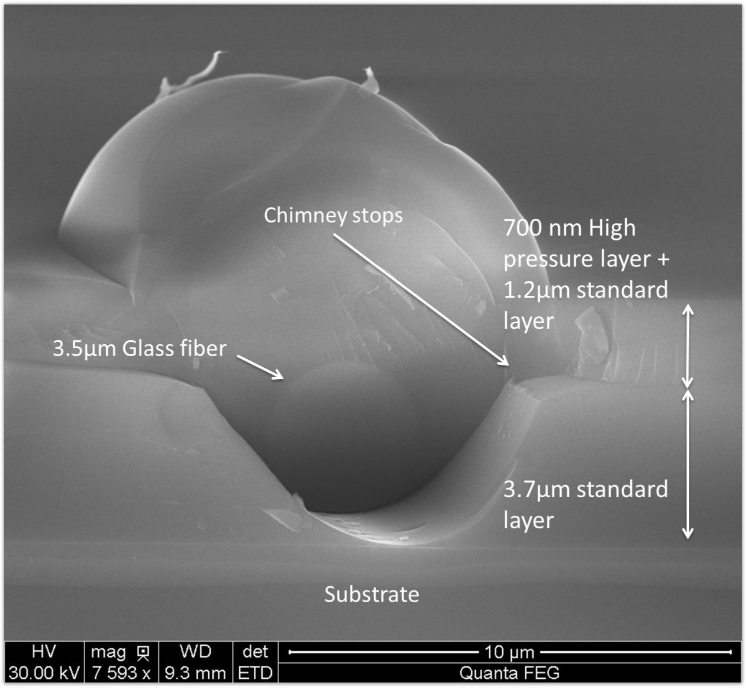

(a) Two portions of the layer are visible at bottom the growth under standard conditions, and at the top the growth under high pressure and under standard conditions. The chimney is sealed as soon as the high pressure growth starts.

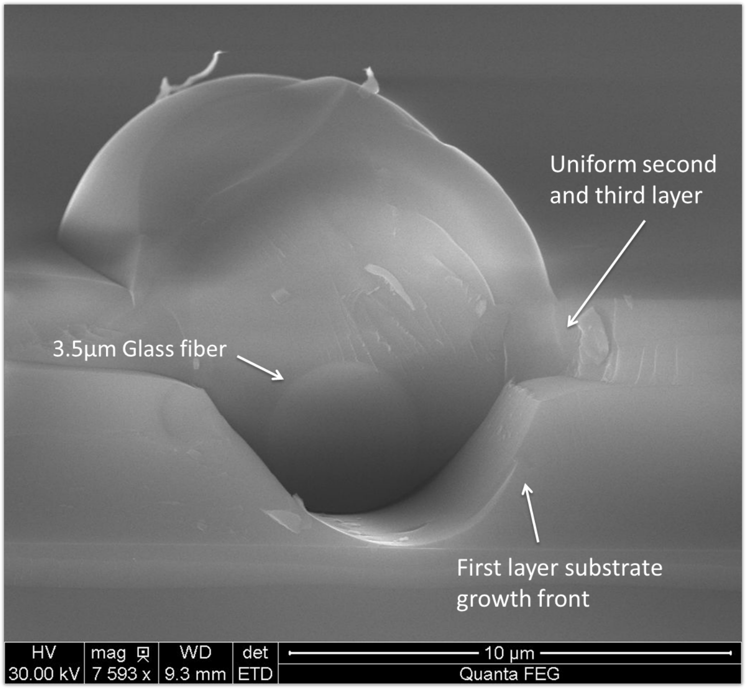

(b) The cleaving plane formed by the chimney shows an uniform contiguous second and third layer.

Figure 6.13: The figure is identical to figure 6.11 and is repeated for discussion - Modulated layer growth of 3.7 µm standard deposition, followed by 700 nm high pressure deposition, and then 1.2 µm standard deposition, encapsulating a 3.5 µm glass fiber.

1. 3.4 μm standard growth: HMDSO 1.16 sccm, oxygen 33 sccm, 110 mT, 70 W, 2.5 hours.
2. Cool for 30 minutes in the atmosphere by venting the chamber.
3. 3.4 μm standard growth: HMDSO 1.16 sccm, oxygen 33 sccm, 110 mT, 70 W, 2.5 hours.
4. Cool for 30 minutes in atmosphere by venting the chamber.
5. 700 nm high pressure growth: HMDSO 1.16 sccm, oxygen 33 sccm, 300 mT, 30 W, 1 hour.
6. 600 nm standard growth: HMDSO 1.16 sccm, oxygen 33 sccm, 110 mT, 70 W, 30 minutes.

As for the previous sample, the cool down steps keep the sample from overheating. The total thickness of the first standard growth is 6.8 μm, which is about the diameter of the glass fiber. Two distinct layers are visible in figure 6.14. The bottom layer is the first 6.8 μm standard growth. The top layer in the image is 1.3 μm thick and consists of the 700 nm high pressure growth and the 600 nm standard growth. A line can be seen along which the growth on the substrate and on the fiber meet. This line corresponds to a weak interface. The chimney would propagate along this weak line if we applied stress that eventually would result in fracture. Once we start growing at high pressure the growth fronts from the substrate and from the top of the particle merge to a uniform blanket layer.

Through experiments on the test 'particles' of T structures and glass fibers we have developed and formulated a three step process for encapsulation. First, standard growth brings the layers that grow on the particle and on the substrate close together. Then high pressure growth makes the film contiguous. The barrier layer then is completed by standard growth. This final portion stays contiguous owing to the underlying high pressure growth. The top standard layer provides the necessary protection against the atmosphere and prevents the permeation of water and oxygen. The thickness of the top standard layer ultimately sets the water permeation property of the entire three layer film.

6.2 Parameters that determine particle encapsulation

This brings us to the question of why the two layers that grow on the substrate and on the particle do not merge initially but merge only after increasing the pressure and lowering the power. To

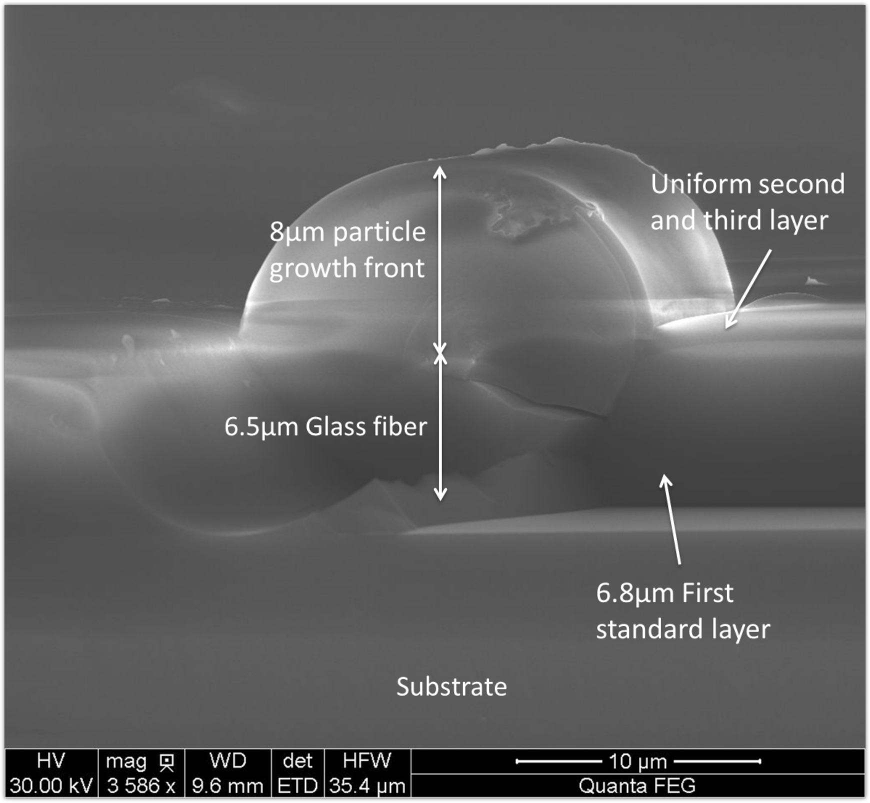

Figure 6.14: Three layer film deposited on a glass fiber: A 6.8 µm standard deposition followed by a 700 nm high pressure deposition and then 600 nm standard deposition encapsulating a 6.5 µm glass fiber.

understand this, we review the several parameters that govern the growth and structure of a layer in PECVD. The parameters that govern the growth of a layer from a gas source and the layers properties, and that come up in any approach to the understanding of layer growth are:

6.2.1 Diffusion of active species in the gas phase

The majority of growth-active species are neutral radicals with thermal energy. They diffuse out of the plasma region, undergoing a small number of collisions before hitting the substrate or another surface in the PECVD reactor. The average distance between collisions is the mean free path.

6.2.2 Directionality of active species in the gas phase

The growth-active species leave the plasma in random directions. In small deposition systems the diameter of the glow discharge may be only a small multiple of the mean free path, in particular at low gas pressure. Then the flux of arriving particles clusters around the normal to the substrate surface. We define angle of incidence of an active species by the variable θ. Normal incidence is defined as angle $\theta = 0$.

6.2.3 Sticking Coefficient of incident active species on the deposition surface

The sticking coefficient α describes the fraction of growth-active species that upon impact sticks to the substrate surface. The fraction that bounces off the surface is $1 - \alpha$. The latter will hit another surface. Its probability of sticking there again is α. One result is that the probability of survival of a growth species after n surface impacts is $(1 - \alpha)^n$. Usually species that do not stick leave the surface in random directions. This makes a given surface element function as a source of species with a flux intensity proportional to the cosine of the angle with the surface normal. A low sticking coefficient α is favorable to covering surfaces that do not face the plasma directly.

6.2.4 Surface diffusion of active species

A reactive species that sticks to the surface may not become immediately incorporated in its permanent position. Instead, while bound to the surface it may diffuse for some time/distance before finding its permanent position. Long surface diffusion enables coverage of surfaces that do not face the plasma. This surface diffusion also is a search for the lowest-energy position. Therefore the longer the search, the more stable the resulting layer.

Each of these parameters affect the profile of the deposited hybrid layer and hence the encapsulation. In many systems it has been shown that increasing the pressure reduces the sticking coefficient, [65, 66, 67]. Furthermore, simulations have shown that sticking coefficient plays a significant role in trench filling. As the sticking coefficient reduces, trench filling becomes more pronounced [68]. Being an inclined trench, the chimney is shadowed by the layer that grows on the particle. As the pressure is increased the chimney is filled.

6.3 Monte-Carlo simulations

To understand the mechanism behind the growth profile, a simulation test bench is developed to understand physically what happens to the active species when we change the deposition conditions. Simulations help us understand and identify the direction in which the recipe has to be modified to lessen the width of chimney quickly. From comparison of SEM micrographs of layer cross sections with cross sections obtained from modeling we estimate values for active species diffusion length, active species directionality, sticking coefficient and surface diffusion length. Used in the model, these parameters then enable us to predict the film profiles obtained under specific growth conditions. Even more important, we will be able to predict how certain shapes of particles will be enveloped by the barrier layer. Similar models have been developed [63, 64, 69].

6.3.1 Simulation test bench

To identify the effects of each of these parameters, a two dimensional numerical simulation test bench based on Monte Carlo method is set up in Matlab. The simulator works by depositing one active species at a time. The simulation starts with a dust particle on the substrate which we define in the simulation window. The particle can be of any shape and size. An active species arrives from the top of the simulation window, originating at a random point and moving downwards at a random angle. The angle at which it arrives on the substrate is given by an active species directionality distribution. For a typical experiment, a cosine distribution is followed. The probability of the particle coming perpendicular to the substrate is the highest. As the angle between the perpendicular to the substrate and the incidence angle increases, the probability falls with the cosine of the angle. Upon contact, the active species stick with a probability given by the sticking coefficient α. The species that do not stick are scattered in at a random angle away from the surface, hit another surface on which they stick or not, etc. Once attached to the surface, the active species moves over a distance given by the diffusion length and is bonded permanently. The process repeats for the next active species until the required height of deposition is achieved.

6.3.2 Sticking coefficient

Figure 6.15 are sample simulation results obtained by setting the sticking coefficient α to 1, 0.8, 0.6, 0.4, 0.2, respectively, on a sample that is a substrate with a T-shaped particle on it. Table 6.1 gives the simulation input parameters. The image window of 14.4 µm by 4.8 µm shows the cross section of the deposited layer. The bottom of the image is the substrate. The grey slab represents the hat portion of the T shaped structure, 500 nm thick and held 1 µm above the substrate. White regions are the deposited hybrid layer, which is approximately 2.5 µm thick. The surface diffusion

Table 6.1: Monte Carlo simulations input parameters. θ is the probability distribution of angle of incoming active species in the simulation.

Simulation		Sticking Coefficient	Directionality	Surface Diffusion length
Sticking Coefficient		0.2,0.4. . . 1	$cos\,(4\theta)$	80 nm
Directionality		1	$cos\,(4\theta)$,$cos\,(3\theta)$, $cos\,(2\theta)$, $cos\,(1.5\theta)$, $cos\,(\theta)$	480 nm
Double Layer	Layer 1	1	$cos\,(4\theta)$,$cos\,(3\theta)$, $cos\,(2\theta)$, $cos\,(1.5\theta)$, $cos\,(\theta)$	480 nm
	Layer 2	1	$cos\,(\theta)$	480 nm

length is set at 80 nm, and both the incoming growth species and the species scattered off the surface follow a cosine distribution:

$$P\,(\theta) = cos\,(4 \times \theta)\,,\ \text{if}\, 4\theta < 90^\circ \tag{6.1}$$

For other θ, $P\,(\theta) = 0$. Equation 6.1 represents a steep incident angle for growth species. The angle of incidence of the incoming species is between $0 \geq \theta \geq 22.5^\circ$ from the normal. From the simulations, we observe that reducing the sticking coefficient gives us a dense film with less columnar growth. The chimney seals faster when the sticking coefficient is lower. The deposition conditions need to be altered in such a way so as to obtain lower sticking coefficient. Reducing the oxygen flow rate is one way to obtain a lower sticking coefficient[70].

6.3.3 Directionality

The directionality of the incoming active species has been modelled. We observe in figure 6.16 that the width of the chimney reduces with increasing directionality. The simulation parameters are given in table 6.1. When multiple layers are deposited, there is a need for the second layer to plug the chimney rapidly. The chimney is plugged faster for a small chimney width. A bilayer deposition is simulated in figure 6.17 where the directionality of the bottom layer is altered while keeping the top layer fixed. The chimney width is minimal when the bottom layer is directional. The chimney is plugged by a second layer with a broad cosine distribution, figure 6.17e.

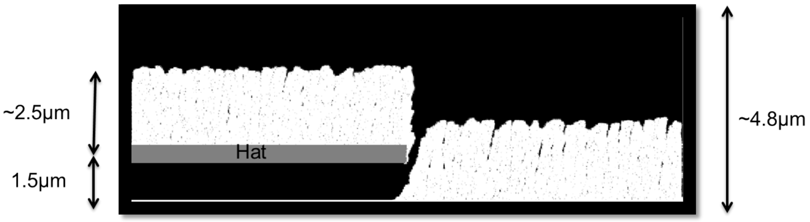

(a) Sticking coefficient = 1.

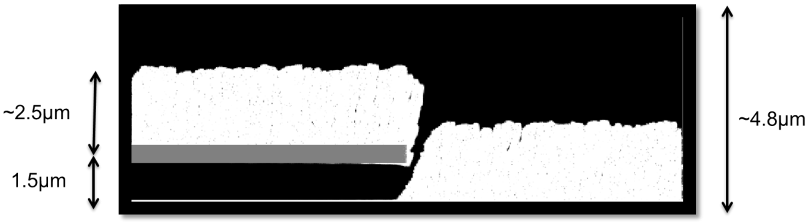

(b) Sticking coefficient = 0.8.

(c) Sticking coefficient = 0.6.

(d) Sticking coefficient = 0.4.

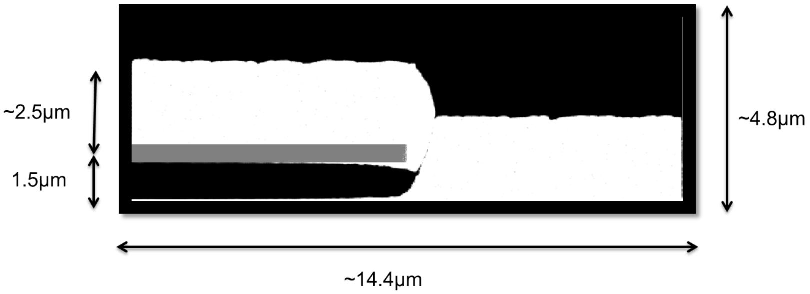

(e) Sticking coefficient = 0.2.

Figure 6.15: Monte Carlo simulation profile of deposition for sticking coefficients 1, 0.8, 0.6, 0.4 and 0.2 respectively. The structure is similar to the T shaped particle. The deposition parameters are: Surface diffusion length = 80 nm, Probability density of active species as a function of angle $P(\theta) = cos(4 \times \theta)$, where $\theta = 0$ is normal incidence.

(a) $P(\theta) = cos(\theta)$ (b) $P(\theta) = cos(1.5\theta)$ (c) $P(\theta) = cos(2\theta)$

(d) $P(\theta) = cos(3\theta)$ (e) $P(\theta) = cos(4\theta)$

Figure 6.16: Monte Carlo simulation profile of depositions with changing directionality of the incoming active species. The sticking coefficient is 1 and surface diffusion coefficient is 480 nm. Probability density of active species as a function of angle $P(\theta)$. $\theta = 0$ is normal incidence.

The deposition recipe determines the parameters of growth. Simulations can serve as guidelines for determining the recipe modification steps to obtain the required growth profile.

6.4 Conclusion

Encapsulating a particle is more complicated than it appears at first sight because of the shadowing effect of the particle. Even when a barrier layer is grown thicker than the particle size an open chimney may result in a break in the encapsulation. The chimney needs to be plugged in the shortest possible deposition time. This is done by increasing the pressure during deposition, which prevents the growth of the chimney. The high pressure layer is held in place by sandwiching between two standard layers. The top standard layer serves two purposes: one, it prevents cracking of the high pressure layer, and two, it does the job of preventing moisture and oxygen permeation. If the size and shape of the biggest particle is known, the thickness of the three layers can be optimized to grow a film in the shortest duration with minimum thickness such that all particles on the device are encapsulated.

(a) Bottom layer: $P(\theta) = cos(\theta)$

(b) Bottom layer: $P(\theta) = cos(1.5\theta)$

(c) Bottom layer: $P(\theta) = cos(2\theta)$

(d) Bottom layer: $P(\theta) = cos(3\theta)$

(e) Bottom layer: $P(\theta) = cos(4\theta)$

Figure 6.17: Monte Carlo simulation profile with two layers of depositions. The two layers have different directionality $P(\theta)$ for the incoming active species. The top layer for all simulations have same directionality, $P(\theta) = cos(4\theta)$. $\theta = 0$ is normal incidence. The bottom layer has changing directionality. The sticking coefficient is 1 and surface diffusion coefficient is 480 nm for both layers.